Deep-Sea Research Part II 166 (2019) 6–18

Contents lists available at ScienceDirect

Deep-Sea Research Part II

journal homepage: www.elsevier.com/locate/dsr2

Holocene monsoon and sea level-related changes of sedimentation in the northeastern Arabian Sea

Nicole Burdanowitz[a,*], Birgit Gaye[a], Lea Hilbig[a], Niko Lahajnar[a], Andreas Lückge[b], Tim Rixen[a,c], Kay-Christian Emeis[a,d]

[a] Institute for Geology, Universität Hamburg, Bundesstraße 55, 20146, Hamburg, Germany
[b] Bundesanstalt für Geowissenschaften und Rohstoffe, Stilleweg 2, 30655, Hannover, Germany
[c] Leibniz-Zentrum für Marine Tropenforschung (ZMT), Fahrenheitstraße 6, 28359, Bremen, Germany
[d] Institute of Coastal Research, Helmholtz Center Geesthacht, Max-Planck-Straße 1, 21502, Geesthacht, Germany

ARTICLE INFO

Keywords:
Arabian sea
Holocene
Indian monsoon
Westerlies
Sediment
Geochemical proxies

ABSTRACT

The Indian Monsoon and the westerlies strongly influence the sedimentation in the northeastern Arabian Sea by impacting rainfall and erosion on land and on biogeochemical processes in the ocean. To disentangle the terrestrial and oceanic processes, we analysed mineralogical and bulk geochemical components of a Holocene sediment core offshore Pakistan. Endmember modelling of grain sizes and principal component analyses (PCA) of major and trace elements identify the origin of sediments and their dominant mode of transport. Sedimentation processes during the early Holocene (10.8–8.2 ka BP) were influenced by the post-glacial sea level rise and orbitally forced strengthening of the Indian summer monsoon (ISM) and westerlies. This led to a shift from rather terrestrial-dominated towards a marine-dominated sedimentation, whereas the fluvial source shifted from the Makran rivers to the Hab River near Karachi. During the mid-Holocene (8.2–4.2 ka BP) a combination of weakening ISM and southward displacement of the ITCZ enhanced the influence of the westerlies, together decreasing river discharges and enhancing aeolian input (probably from the Sistan Basin region). This trend continued during the last ca. 4 ka when the increasing aridification of the Hab River catchment further increased the aeolian inputs. Solar and lunar driven short-term variations as well as Bond events known from the North Atlantic Ocean superpose these trends. They lead to a pronounced increase of fluvial inputs between 8.6–8.4 ka BP and at ca. 3 ka BP as well as to dry events around 4.2 ka and 1.2–1 ka BP. Our study highlights the increasing influence of the westerlies on the sedimentation processes in the northeastern Arabian Sea towards the late Holocene.

1. Introduction

The northeastern Arabian Sea (AS) is located in a critical region where the climate regimes of the Indian summer monsoon (ISM) and of Indian winter monsoon (IWM) influenced by the westerly wind systems overlap. The general concept on past evolution of this interplay is that the ISM and IWM strengths where antiphased (Böll et al., 2014; Caley et al., 2011; Chauhan et al., 2006; Klöcker and Henrich, 2006; Reichart et al., 2002; Resmi and Achyuthan, n.d.; Saher et al., 2007). The ISM strength is linked to the mean annual position of the Intertropical Convergence Zone (ITCZ) and a northward shift of the ITCZ leading to stronger ISM during periods of high northern hemisphere (NH) insolation, such as during the early to mid-Holocene. In contrast, reduced NH insolation leads to weakening of the ISM, as, for instance, during the last glacial maximum (Böll et al., 2014; Caley et al., 2011; Herzschuh, 2006; Wang et al., 2005; Yancheva et al., 2007). In addition to the overriding and long-term orbital influence, forcing from solar variability, El Niño Southern Oscillation (ENSO) and North Atlantic Oscillation (NAO) have been suggested to be responsible for centennial to millennial monsoon strength variability (Böll et al., 2015; Herzschuh, 2006; Wang et al., 2005).

The northeastern AS is a key region to study the Holocene variability of the IWM/westerlies, because the two atmospheric systems are well expressed and overlap. Besides its location, the preservation of climate signals is favoured by an oxygen minimum zone (OMZ) between 200 and ~1200 m water depth (Schott et al., 1970; Schulz et al., 1996; von Rad et al., 1995). The limited oxygen content of the OMZ inhibits bioturbation and, therefore, facilitates the formation of

* Corresponding author.
E-mail address: nicole.burdanowitz@uni-hamburg.de (N. Burdanowitz).

https://doi.org/10.1016/j.dsr2.2019.03.003
Received 15 May 2018; Received in revised form 1 March 2019; Accepted 11 March 2019
Available online 14 March 2019

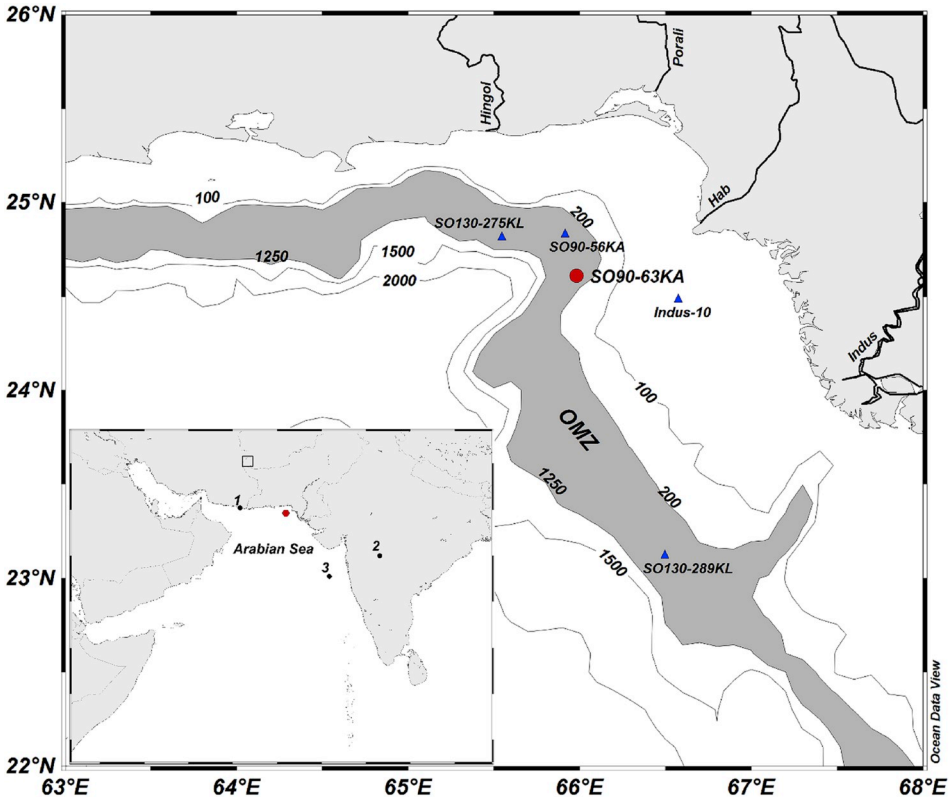

Fig. 1. Map of the study area with the SO90-63 KA core location indicated as red point. The dark shaded area indicated the oxygen minimum zone (OMZ). Core site locations SO90-56 KA, SO130-275 KL, SO130-289 KL and Indus-10 cited are indicated as blue triangles. The black dots indicate core site location of OS73 (1), Lonar lake (2) and core site SK148/55 (3), respectively. The Sistan Basin is marked as a black box in the small map. (For interpretation of the references to colour in this figure legend, the reader is referred to the Web version of this article.)

laminated sediments on the continental margin (Schott et al., 1970; von Rad et al., 1995; von Stackelberg, 1972). The laminated sediments are interrupted by light grey event deposits (C-layers), which are interpreted as suspensate event deposits (von Rad et al., 1999a) or catastrophic flash flood events due to extreme rainfall events in the hinterland and the Makran coast (Lückge et al., 2002). Reconstructions of Holocene sea surface temperature (SST) and primary productivity (Böll et al., 2015, 2014; Munz et al., 2017, 2015), which express IWM strength (Andruleit et al., 2000; Schulz et al., 2002), revealed increasing IWM intensity during the Little Ice Age (LIA) interpreted to signal southward migration of the ITCZ during this cold interval (Böll et al., 2014; Munz et al., 2017, 2015). Although several studies address the Holocene variability of the ISM (e.g. Anoop et al., 2013; Dixit et al., 2014; Fleitmann et al., 2007; Ivory and Lézine, 2009; Menzel et al., 2014; Sarkar et al., 2000; Thamban et al., 2007), the knowledge of the Holocene IWM/westerlies variability is insufficient due to the lack of suitable records and the superposition of the ISM signal on the annual signals recorded in the sediments (Deplazes et al., 2014; Lückge et al., 2001).

Lithogenic material deposited in the northeastern AS is mainly transported by rivers but also by wind as aeolian dust (Deplazes et al., 2014; Kolla et al., 1981; Schulz et al., 1996; Sirocko and Lange, 1991; Stewart et al., 1965; von Rad et al., 1999b, 1995). Whereas the southern part of the northeastern AS (south of Karachi) is dominated by sediment input from the Indus River (e.g., Bourget et al., 2013; Deplazes et al., 2014; Limmer et al., 2012), the Makran rivers (e.g., Hingol River) are the major lithogenic source in the northern AS (Bourget et al., 2011, 2010; Lückge et al., 2001; Staubwasser and Sirocko, 2001; Stow et al., 2002). Limmer et al. (2012) reported Hab River input to the northern Indus shelf during the early Holocene low sea level. At around 8 ka BP, a shift to more Indus River derived sediment deposition is indicated, which is related to the Holocene sea level rise (Limmer et al., 2012). Considering that the Indus River is influenced by meltwater discharge and summer monsoon precipitation (Bookhagen and Burbank, 2010; Karim and Veizer, 2002; Lückge et al., 2012; Lutz et al., 2014; von Rad et al., 2002) and that the region of the Makran river catchments receives a high amount of precipitation during the winter (Lückge et al., 2001; von Rad et al., 2002), changes of the sediment provenance may reveal changes of the ISM and westerly derived precipitation.

The Sistan region (southeastern Iran) is a major dust source for the northern AS, Pakistan and Afghanistan (Alam et al., 2011; Kaskaoutis et al., 2014; Rashki et al., 2012). Sistan dust is transported by northerly winds, the so called Levar wind, which blow from June to September. The Levar winds are driven by a high pressure gradient between low pressure cell over Pakistan and high pressure cell over west central Asia (Kaskaoutis et al., 2015a, 2015b; Rashki et al., 2012). Dust supply is not only restricted to the timing of the Levar wind, but also occurs during the winter and pre-monsoon season when northeasterly and westerly winds prevail over the region (Pease et al., 1998; Rashki et al., 2017; Sirocko and Lange, 1991; Tindale and Pease, 1999). Back trajectory studies reveal the importance of dust sources in the desert regions in northwestern India as well as north of the Makran coast (Hussain et al., 2005; Pease et al., 1998; Rashki et al., 2015; Tindale and Pease, 1999). Changes in the ISM and IWM strengths, expressed in precipitation as well as wind, thus lead to shifts in the source of aeolian, and fluvial input and in aeolian versus fluvial fractions of sedimentary deposits on the northern AS margin.

Here a high-resolution sedimentary record from the northeastern Arabian Sea OMZ is examined to reconstruct changes in the Holocene sedimentation processes off Pakistan. Data sets of grain sizes, major and trace elements, stable isotopes of bulk carbonates as well as total organic carbon (TOC) and nitrogen (N) contents and stable nitrogen isotopes are analysed to identify the origin of the sediments deposited since the early Holocene. Due to its location, the sediment core provides a scarce and valuable paleoclimate archive to study the Holocene interaction of the Indian monsoon and westerlies realm.

2. Material and methods

Box core SO90-63 KA was retrieved from the northeastern Arabian Sea off Pakistan (24°36.6′N, 65°59.0′E, 316 m water depth) during the RV SONNE cruise SO90 in 1993 (Fig. 1). The chronology of SO90-63 KA has been published by Staubwasser et al. (2003, 2002) and is based on 80 ^{14}C dating of planktonic foraminifers *Globigerinoides sacculifer*. The 697 cm long core, with the upper 18 cm missing, covers the last ca. 10,800 years and therefore most of the Holocene period (Staubwasser et al., 2003, 2002). It has to be noted that the core has partly dried out and shrank of about 12% between 540 and 584 cm (corresponding to the time interval ca. 8.5–9.3 ka BP). Therefore, a correction of the core depth was necessary. In total, 202 samples with an averaged temporal resolution of ca. 5–240 years were analysed for nitrogen, organic carbon and carbonate contents and stable nitrogen isotopes. This sample set includes separately sampled white C-event layers. We used 123 (temporal resolution of ca. 5–710 years) and 35 samples (temporal resolution of ca. 5–970 years) for XRF elemental and grain size analyses, respectively.

2.1. Bulk analyses (nitrogen, organic carbon, carbonate)

All samples were freeze-dried and homogenized using an agate mortar and pestle prior to chemical treatment and analysis. Total carbon (TC) and nitrogen were analysed with a Euro EA3000 elemental analyser. Duplicate measurements yielded a precision of 0.13% and 0.02% for total carbon and nitrogen, respectively. Samples for the measurement of total organic carbon (TOC) were treated with 1 *M* hydrochloric acid (HCl) prior to instrumental analysis in order to remove inorganic carbon. TOC was analysed with a Euro EA3000 elemental analyser with a precision of 0.25%. The carbonate carbon was calculated as the difference of TC and TOC.

2.2. Stable nitrogen isotope analysis

The stable nitrogen isotopes ($\delta^{15}N$) were analysed using an Elementar IsoPrime 100 isotope ratio mass spectrometer after high-temperature combustion in an Elementar CHNOS Vario isotope elemental analyser at 950 °C. Pure tank nitrogen was calibrated against the International Atomic Energy Agency reference standards IAEA-N1 and IAEA-N2 and used as working standards in addition to an internal standard. Replicate measurements of the reference standards yielded a precision of better than 0.2‰. Duplicate measurements of the samples resulted in a mean standard deviation of 0.05‰.

2.3. Stable carbon and oxygen isotope analysis of bulk carbonate

The bulk carbonate stable carbon ($\delta^{13}C_{carb}$) and oxygen isotopes ($\delta^{18}O_{carb}$) of the freeze-dried and homogenized samples were analysed at Center for Marine Environmental Sciences (MARUM, University of Bremen) using a Finnigan MAT 251 gas isotope mass spectrometer with a Kiel I automated carbonate preparation device. The analytical precision based on replicate measurements (n = 35) of the house standard (Solnhofen Limestone calibrated against NBS19) was 0.03‰ and 0.04‰ for $\delta^{13}C_{carb}$ and $\delta^{18}O_{carb}$, respectively. All $\delta^{13}C_{carb}$ and $\delta^{18}O_{carb}$ values are reported in ‰ against Vienna Pee Dee Belemnite (VPDB).

2.4. XRF elemental analysis

Freeze-dried and homogenized samples were analysed for their elemental composition using X-ray fluorescence (XRF) analyses. The XRF measurements were conducted at Bundesanstalt für Geowissenschaften und Rohstoffe (BGR, Hannover) using Philips PW 1400 and Philips PW 1480 instruments. 42 major and trace elements were quantitatively analysed after fusion of the samples with Lithiummetaborate at 1200 °C for 20 min (sample/$LiBO_2$ = 1/5). Quality of the results was controlled with certified reference materials (CRM) (i.e., BCR, Community Bureau of Reference, Brussels). The precision for major elements was generally better than ± 0.5% and better than 5% for trace elements.

2.5. Grain size analysis

Grain size analyses were conducted at the Center for Tropical Marine Research (ZMT, Bremen). 250 mg of bulk sediment were treated with HCl and hydrogen peroxide (H_2O_2) to remove inorganic carbon and organic matter (e.g. Sun et al., 2002). Thereafter, Calgon® ($Na_6P_6O_{18}$) was added and boiled to avoid particle coagulation. The grain sizes were measured using a Horiba LA-950V2 laser scattering particle size analyser. Each sample was measured in triplicate and results were averaged. Grain size distributions were calculated for 93 grain size classes between 10 nm and 3 mm. Grain size distribution parameters were calculated with GRADISTAT V.8. End-member modelling were conducted by using an end-member modelling analysis (EMMA) script for Matlab (Dietze et al., 2012).

2.6. Aerosol grain size distribution data

The aerosol grain size distribution data for Karachi were obtained from the Aerosol Robotic Network (AERONET, https://aeronet.gsfc.nasa.gov/new_web/index.html) program based on ground-based remote sensing measurements of aerosols using sun photometer (Holben et al., 2001, 1998). We used the monthly averaged aerosol size distribution (2006–2017, almucantar level 1.5) of the aerosol inversion version 2 product. Monthly averaged data of each single year were averaged as monthly mean for 2006–2017. We then used the mean grain size distribution of the months June–September, as during this time period the Levar wind, which is responsible for dust storms in the Sistan region and blowing dust to our study area, is strongest. For dust during the winter we used the mean grain distribution of the months November–March.

3. Results

3.1. Bulk and stable nitrogen analyses

The analyses of N, TOC and carbonate exhibit clear differences between 'normal' sediments and C-event layer sediments (Table 1). The C-event layers have consistently lower N (0.14 ± 0.06%), TOC (1.00 ± 0.59%) and carbonate (16.1 ± 2.8%) contents than the sediments (N: 0.23 ± 0.06%; TOC: 1.87 ± 0.46%; carbonate: 19.5 ± 4.0%). The $\delta^{15}N$ values are slightly heavier in the sediments (8.1 ± 0.5‰) than in the C-event layers (7.7 ± 0.7‰). A general increase in TOC content is observed from early (0.7%) to late Holocene (2.6%) with phases of higher TOC values around ca. 8.3 ka BP, 6.8–7.5 ka BP, 3.9–4.2 ka BP and 1.2–2.0 ka BP as well as increasing TOC values since the last ca. 0.6 ka (Fig. 2). The N content of the sediment core

Table 1
Mean values of concentrations, grain size as well as $\delta^{13}C_{carb}$ and $\delta^{18}O_{carb}$ for sediments and C-event layers of sediment core SO90-63 KA. The numbers of samples (n) are given in brackets.

	Sediments	C-layers
N (%)	0.23 ± 0.06 (n = 184)	0.14 ± 0.06 (n = 14)
TOC (%)	1.87 ± 0.46 (n = 184)	1.00 ± 0.59 (n = 14)
Carbonate (%)	19.5 ± 4.0 (n = 184)	16.1 ± 2.8 (n = 14)
$\delta^{15}N$ (‰)	8.1 ± 0.5 (n = 183)	7.7 ± 0.7 (n = 14)
Mean median grain size (μm)	6.1 ± 1.1 (n = 21)	8.1 ± 4.4 (n = 14)
$\delta^{13}C_{carb}$ (‰ VPDB)	−0.81 ± 0.42 (n = 40)	−1.32 ± 0.52 (n = 13)
$\delta^{18}O_{carb}$ (‰ VPDB)	−3.28 ± 0.71 (n = 40)	−4.83 ± 1.30 (n = 13)

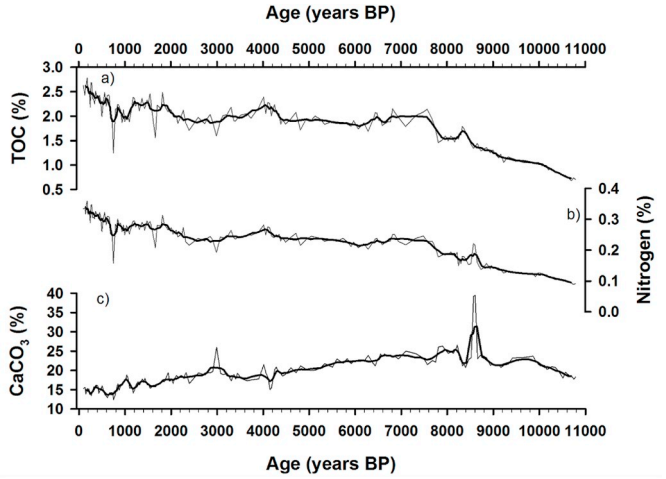

Fig. 2. a) Total organic carbon (TOC), b) nitrogen and c) calcium carbonate content ($CaCO_3$) of SO90-63 KA. Thick black lines indicate five-point running average.

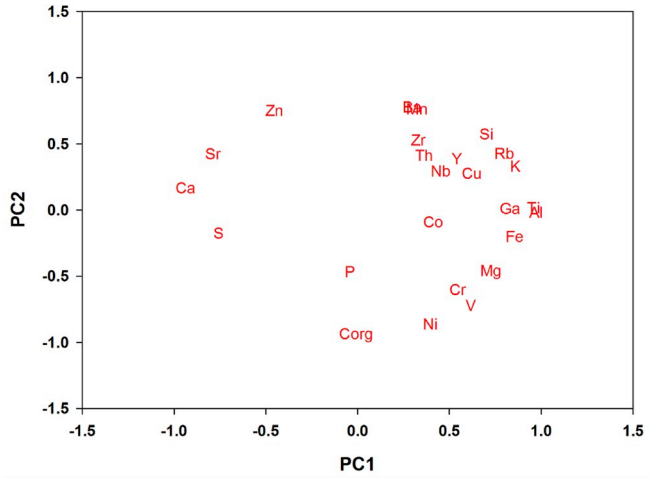

Fig. 3. Plot of the first and second axis of principal component analysis using the elemental composition of the SO90-63 KA sediments.

reveals a similar pattern as TOC with a general increase from the early to late Holocene. In contrast, the carbonate content decreases from the early to late Holocene. Intervals with higher carbonate contents are observed at ca. 8.5–8.6 ka BP, 7.8–8.2 ka BP, 2.8–3.2 ka BP and around 1 ka and 0.4 ka BP (Fig. 2). The $\delta^{15}N$ values vary between 7.9 and 8.4‰ from 10.8 to 8.8 ka BP and show a gradual decrease of $\delta^{15}N$ to 7.1‰ until 7.8 ka BP: An interval of more depleted $\delta^{15}N$ (7.1–7.5‰) occurred between 7.8 and 6.2 ka BP. From 6.2 ka BP to recent a gradual increase of $\delta^{15}N$ values up to 9‰ are observed.

3.2. Stable carbon and oxygen isotopic composition of bulk carbonate

As for the bulk parameters, $\delta^{13}C_{carb}$ and $\delta^{18}O_{carb}$ analyses differ between sediments and C-event layers (Table 1). Overall, C-event layers are more depleted in $\delta^{13}C_{carb}$ (-1.32 ± 0.52‰) and $\delta^{18}O_{carb}$ (-4.83 ± 1.30‰) than the sediments with $\delta^{13}C_{carb}$ and $\delta^{18}O_{carb}$ values of -0.81 ± 0.42‰ and -3.28 ± 0.71‰, respectively.

3.3. XRF analysis

SiO_2 is the major constituent of sediments (43 ± 1.4%) and C-event layers (48% ± 3.3%) followed by Al_2O_3 (sediments: 13 ± 0.8%, C-event layers: 14 ± 0.8%) and CaO (sediments: 11.3 ± 2.0%, C-event layers: 8.8 ± 1.2%) (Suppl. Table). Further, moderate amounts of Fe_2O_3 (sediments: 5.6 ± 0.4%, C-event layers: 5.8 ± 0.5%) and MgO (sediments: 3.4 ± 0.1%, C-event layers: 3.4 ± 0.3%) are detected, whereas the amounts of K_2O, Na_2O, TiO_2, SO_3, P_2O_5 and MnO are below 2%.

For statistical analysis we conducted a principal component analysis (PCA) of the elemental composition of the sediments (Fig. 3, Fig. 4). It has to be noted that high-resolution major and trace elemental data already existed for the lower part of core (400–697 cm, Staubwasser, 1999). Comparing the two data sets of the lower part of the core (400–697 cm) shows that the trend of most of the elemental ratios (Sr/Ca, Ti/Al, Mg/Al, Mn/Al, Fe/Al) is similar in both data sets (Suppl. Fig. A1). Differences in the Zr/Al ratios are due to incomplete recovery of the analytical method for Zr used by Staubwasser (1999). The author stated that the recovery of his analytical method is about 54% (Staubwasser, 1999). For comparison, we conducted a PCA for each data set from the lower part of the core (400 cm to bottom) and analysed elements which are common in both data sets unaffected by incomplete recovery (Suppl. Fig. A2). Apart from small differences of Cu, Cr and Zn, the PCA elements common to both data sets are similar. However, despite the issue of different analytical methods, some elements (e.g., Co, K, Nb, P, S, Si) are not available in the older data set for the core, so that we could not include the data set of Staubwasser (1999) in the PCA. The PCA exhibits that the first two components describe 66.5% of the total variance in the Holocene sediments of SO90-63 KA (Table 2). The first and second components describe 41.1% and 25.4% of the variance, respectively. The first component reveals two different clusters with negative loadings on Ca, C_{org}, P, S, Sr and Zn as well as positive loadings on Al, Ba, Co, Cr, Cu, Fe, Ga, K, Mg, Mn, Nb, Ni, Rb, Si, Th, Ti, V, Y and Zr. The second component exhibits positive loadings on Ba, Ca, Cu, K, Mn, Nb, Rb, Si, Sr, Th, Y, Zn and Zr and negative loadings on Co, C_{org}, Cr, Fe, Mg, Ni, P, S and V (Fig. 3).

3.4. Grain size analysis

The grain size analyses of the sediments reveal a unimodal distribution pattern (Fig. 5) with median grain sizes between 4.9 and 8.6 µm (mean: 6.1. ± 1.1 µm, Table 1). Coarser grain sizes (up to 8.6 µm) characterise the early Holocene that shift to finer grain sizes (~4.9 µm) towards the late Holocene (Suppl. Fig. A3). C-event layers are of unimodal distribution (Fig. 5) with coarser grain sizes of 4.9–22.0 µm (mean: 8.0 ± 4.4 µm, Table 1) than the sediments. The EMMA of the sediments reveals three main end-members (Fig. 6). End-member 1 (EM1) has a trimodal distribution with modal grain sizes of 14.2 µm, 4.2 µm and 42.1 µm. In contrast, end-member 2 (EM2) has a bimodal distribution with modal grain sizes of 14.2 µm and 0.3 µm, end-member 3 (EM3) has a unimodal distribution with a modal grain size of 3.7 µm.

EM3 has an inverse trend compared to the Zr/Al as well as the Mg/Al ratios throughout the Holocene (Fig. 7) and median grain size and Zr/Al ratios of sediments are significantly correlated ($r = 0.73$, $p < 0.001$, $n = 16$).

4. Discussion

4.1. Source of sediments and sedimentation processes

The results of the PCA are interpreted with respect to the element sources. The two clusters of elements of the first component in the PCA distinguish different sediment sources (Fig. 3). The significant positive correlation ($r = 0.87$; $p < 0.001$, $n = 111$) of Ca and Sr (Suppl. Fig. A4) indicates a marine source of $CaCO_3$. Earlier studies found that Sr and Ca are mainly derived from biogenic carbonates in the northern Arabian Sea (Reichart et al., 1997; Shimmield and Mowbray, 1991; von Rad et al., 2002). While a high Sr content is linked to high production and/or preservation of aragonite containing pteropod shells

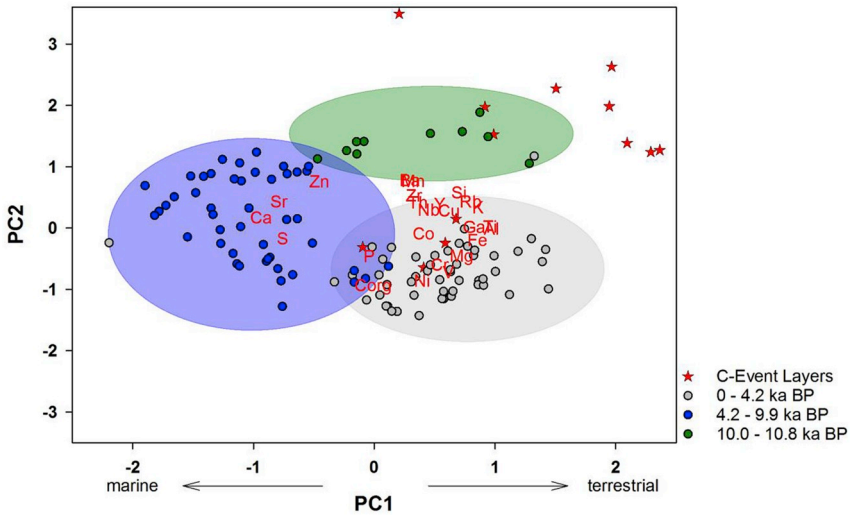

Fig. 4. Plot of the first and second axis of principal component analysis using the elemental composition of the SO90-63 KA sediments. C-event layers are marked as red stars and sediments as dots. Big shaded circles indicate different age intervals of sediments with intervals from 10.8 to 10 ka BP (green), from 9.9 to 4.2 ka BP (blue) and from 4.2 ka BP to modern (grey). (For interpretation of the references to colour in this figure legend, the reader is referred to the Web version of this article.)

Table 2
PCA results of the SO90-63 KA sediments.

Component	Eigenvalue	Variance (%)	Cumulative (%)
PC1	10.28	41.13	41.13
PC2	6.34	25.35	66.48

(Sutherland et al., 1984; von Rad et al., 1999b), enhanced Ca content indicates higher productivity of $CaCO_3$-containing organisms, such as coccoliths or foraminifera.

Aluminosilicates such as Al, K, Rb or Ti are typical components of clay detritus derived from the continent (Rashki et al., 2013; Shimmield and Mowbray, 1991; Sinha et al., 2006; Sirocko et al., 2000). Therefore, we conclude that positive loadings of PC1 of the aluminosilicate group represents higher abundance of material of terrestrial origin, whereas negative PC1 loadings of Ca, Cl, S, Sr and Zn represent higher abundance of marine matter (Figs. 3 and 4).

The good correlation between the Zr/Al ratio and the median grain size of the sediments is a reflection of zirconium often being associated with heavy minerals of coarser grain sizes (Dypvik and Harris, 2001; Fralick and Kronberg, 1997; von Rad et al., 1999b). Therefore, the Zr/Al ratio can be used as a grain size indicator (Deplazes et al., 2014). Further, Lückge et al. (2001) found high Zr/Al ratios in Hingol River sediments and in thick varved marine sediments on the adjacent continental margin attributing this to its fluvial source and increasing transport energy.

Lithogenic material in the study area is derived from fluvial input of the Makran rivers (e.g. Hingol, Hab; Forke et al., 2019; Lückge et al., 2002; Staubwasser and Sirocko, 2001; Stow et al., 2002; von Rad et al., 1999a). Bela ophiolites in southern Pakistan are located within the draining area of the Makran rivers and their elemental composition (SiO_2: 42.0–78.8%; CaO: 0.8–17.0%; Al_2O_3: 10.6–21.1%) varies over large ranges (Ahmed, 1993; Ahmed and Ernst, 1999). Dust storms in the Sistan region have been reported to increase the sediment input considerably (Alam et al., 2011; Kaskaoutis et al., 2015b, 2014; Rashki et al., 2012). The elemental composition of dust (SiO_2: 46.8–47.8%; CaO: 12–12.2%; Al_2O_3: 10.4–10.8%) in the Sistan region (Rashki et al., 2013) is similar to that found in the SO90-63 KA sediments. The average grain sizes of dust from the Sistan region are, in general, larger in the summer months than during winter due to stronger winds and the resulting dust mobilisation (Rashki, 2012). Dust storms over Karachi during the Levar wind months (June–September) exhibit median grain sizes of 2.5 μm and modes of about 2.6 μm (Fig. 5), respectively. Dust transported during the winter season has similar median grain sizes of 2.4 μm but modes of 3.4 μm and 0.2 μm (Fig. 5). Both fall in a range which is rather indicative of a distal than a proximal aeolian dust source (Mahowald et al., 2014, 2005; von Rad et al., 2002).

In contrast, material from the Hingol River is coarse (median grain sizes of 9.1 μm) and has modes of about 9.5 μm and 42.1 μm (Forke et al., 2019). The mode of 9.5 μm is interpreted as suspended material of the river, whereas the mode 42.1 μm is interpreted as river bed load material (Forke et al., 2019). The median grain sizes of the SO90-63 KA sediments (6.1 ± 1.1 μm) and C-event layers (8.1 ± 4.4 μm) are in the range between aeolian dust and Hingol River sediments. The modal grain sizes of EM1 (14.2 μm and 42.1 μm) are in the range of those from the Hingol River suspension (9.5 μm) and bed load material (42.1 μm), respectively and are in line with end-member analyses of SO130-275 KL (Forke et al., 2019). Therefore, EM1 can be used as an indicator for fluvial input. In contrast, EM3 (mode: 3.7 μm) probably reflects aeolian dust input. EM2 (mode: 14.2 μm) suggests a mixed signal of fluvial and aeolian input (McCave, 1972).

The majority of the C-event layers in the core are clearly associated with the terrestrial aluminosilicate group corroborating earlier studies suggesting their terrigenous, non-biogenic origin (Lückge et al., 2002; Schulz et al., 1996; von Rad et al., 2002, 1999a). Lückge et al. (2002) reported lower percentages of biogenic compounds in C-event layers compared to 'normal' sedimentation layers, which agrees with in our record (Table 1). Further, more depleted bulk $\delta^{13}C_{carb}$ and $\delta^{18}O_{carb}$ in the C-Event layers than in the 'normal' sediment layers indicate a different source of carbonate in the C-Event layers, as was recently reported for bulk $\delta^{13}C_{carb}$ in the nearby core SO130-275 KL (Forke et al., 20198). $\delta^{13}C$ and $\delta^{18}O$ of planktic foraminifera in core SO90-63 KA are, on average, more enriched ($\delta^{13}C = 0.89 \pm 0.15$‰, $\delta^{18}O = -1.92 \pm 0.15$‰; Staubwasser, 1999; Staubwasser et al., 2003) than bulk $\delta^{13}C_{carb}$ and $\delta^{18}O_{carb}$ in both, C-event layers and 'normal' sediment layers (Table 3). Coccolith $\delta^{13}C$ (0.13 ± 0.80‰) and $\delta^{18}O$ (−0.77 ± 0.91‰) from the tropical southern Atlantic are also more enriched than bulk carbonate in SO90-63 KA (Fink et al., 2010). This contrasts with terrestrial pedogenic carbonates in western India and Pakistan that are, on average, more depleted in $\delta^{13}C_{carb}$ (−3 to −8‰) and $\delta^{18}O_{carb}$ (−1 to −5‰, Table 3) (Cerling and Quade, 1993; Laskar et al., 2013). The bulk carbonate isotopes of the C-Event layers lie between those of marine and terrestrial carbonates, but tend to have a more terrestrial signal than the sediments of SO90-63 KA.

Coarse grain sizes and high Zr/Al ratios in sediments suggest higher transport energy prior to deposition than sediments with lower Zr/Al ratios. Altogether, our data corroborates earlier studies that these event layers are deposited under high transport energy probably due to river flood events or turbidites of reworked terrestrial sediments from the slope (Forke et al., 2019; Lückge et al., 2002; Stow et al., 2002; von Rad

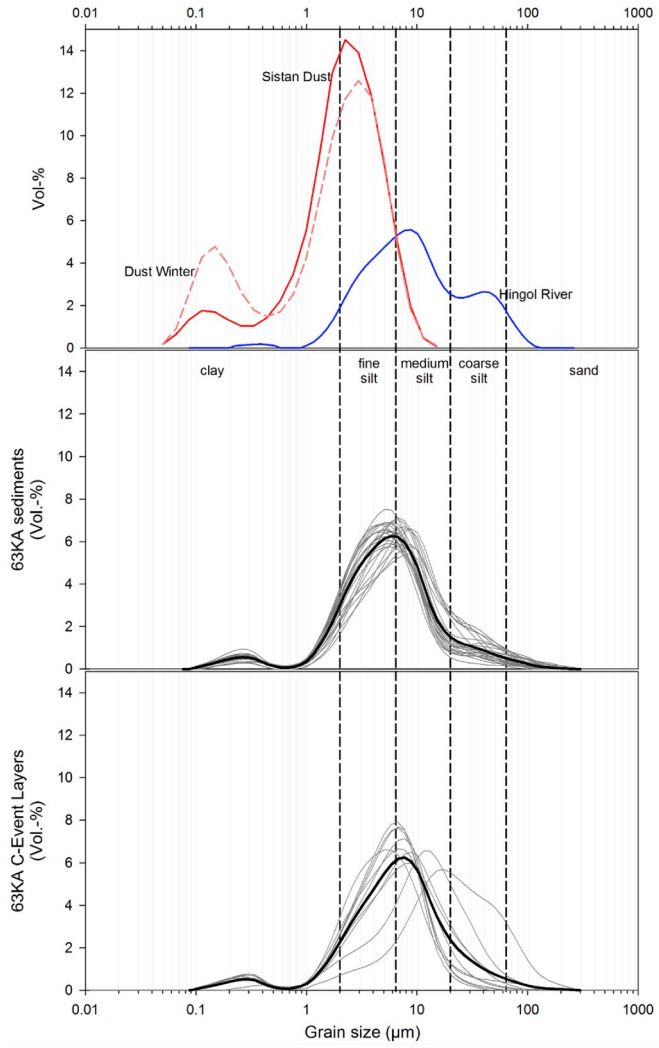

Fig. 5. Mean grain size distribution of SO90-63 KA sediments and C-event layers (black bold lines). Grain size distributions of individual samples are shown in grey. Further, aerosol grain size distribution of "Sistan dust" (red line, June–September) and "winter dust" (dashed red line, November–March) are shown. The aerosol data include averaged monthly grain size distributions from 2006 to 2017 for Karachi (Pakistan) and obtained from the Aerosol Robotic Network (AERONET, https://aeronet.gsfc.nasa.gov/new_web/index.html; Holben et al., 2001, 1998). The blue line indicates the mean grain size distribution of lower Hingol River flood terraces (Forke et al., 2019). (For interpretation of the references to colour in this figure legend, the reader is referred to the Web version of this article.)

et al., 2002).

4.2. Change of sedimentation processes from early to mid- and late holocene

The sedimentological and geochemical patterns observed downcore and through time agree with the division of the Holocene into early (11.7–8.2 ka BP, stage III), mid- (8.2–4.2 ka BP, stage II) and late Holocene (4.2 ka BP – recent, stage I; Walker et al., 2012) (Fig. 7).

One driver of these changes in sedimentation was sea level that rose about 60–80 m since the Younger Dryas (Hashimi et al., 1995; Siddall et al., 2003). The rapid sea level rise of about 40 m (Hashimi et al., 1995; Siddall et al., 2003) during the early Holocene is partly responsible for the pronounced changes of the elemental ratios (e.g., Sr/Ca, Mg/Al, Ti/Al) as well as other bulk parameters in SO90-63 KA (Figs. 7 and 8) during stage III. The increase to coarser grain sizes (Zr/Al, EM3) from 10.8 ka BP to ca. 8.2 ka BP suggest a shift in the

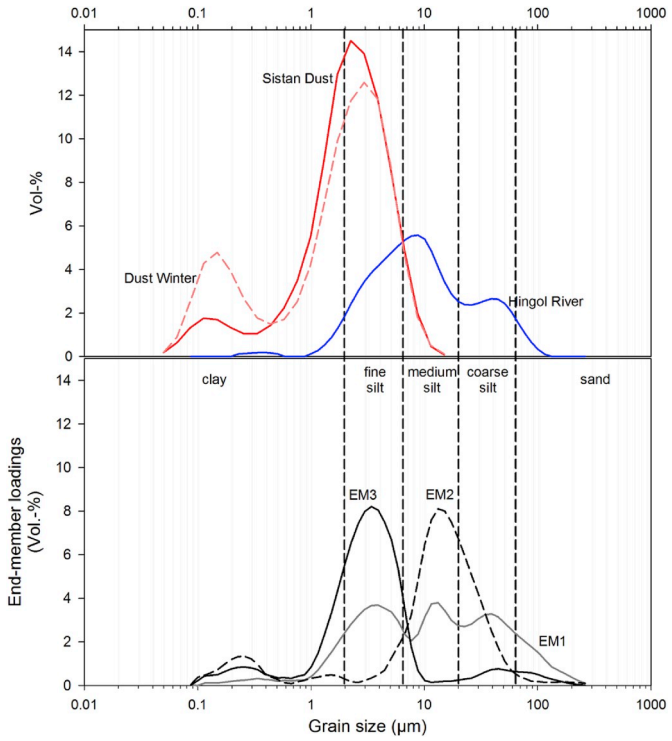

Fig. 6. Comparison of grain size distributions for aeolian Sistan dust and winter dust as well as lower Hingol River flood terraces with modelled end-members of SO90-63 KA sediments.

terrestrial fraction towards relatively more fluvial compared to aeolian input, partly as a result of more humid condition during this time period (Fleitmann et al., 2007; Herzschuh, 2006). The early Holocene was characterized by strong ISM precipitation and winds caused by a northward shift of the ISM due to maximum summer insolation (Demske et al., 2009; Dixit et al., 2014; Hamzeh et al., 2016a; Herzschuh, 2006; Prasad and Enzel, 2006; Rawat et al., 2015; Sirocko et al., 2000; Thamban et al., 2007). This has led to increasing river discharges draining the NW Himalayas and Hindu Kush region (Alizai et al., 2011; Clift et al., 2008; Giosan et al., 2012; Hamzeh et al., 2016a; Srivastava et al., 2017). At that same time, PC1 in our record indicates a shift towards more marine input lasting until ca. 8.2 ka BP which can be partly attributed to an increasing distance to the coast due to sea level rise. However, not only the distance to the coast has changed. Although the core site is recently located near the river channel system including the Hab, Porali and Phor rivers with the Hab River as the dominant sediment contributor, the Hingol River was an important sediment contributor during the early Holocene (Bourget et al., 2011, 2010). The Porali River has discharged directly into the Arabian Sea during the early Holocene, whereas it drains into the Miani Hor lagoon acting as a sediment buffer and hindering direct sediment delivery to the Arabian Sea today (Bourget et al., 2010). Cr/Cu ratios from core SO90-63 KA are in between of those from surface sediments of the northern Arabian Sea and the Indus River area (Staubwasser, 1999; Staubwasser and Sirocko, 2001). Even further south, the Indus-10 record located at the western shelf of the Indus River Canyon is a mixture of Indus River derived sediments and ophiolite sourced materials transported from the north by the Hab River with the latter as a result of low sea level (Limmer et al., 2012).

The Sr/Ca ratios show a significant change during stage III compared to the stages II and I. Highest Sr/Ca ratios are observed between ca. 9.8 and 9.4 ka BP and decrease until ca. 8.4 ka BP (Fig. 7f). This was also found in the high-resolution measurements of the lower section of the sediment core (Staubwasser, 1999) (Suppl. Fig. A1). Sr is mostly associated with aragonite produced by shallow-water aragonitic

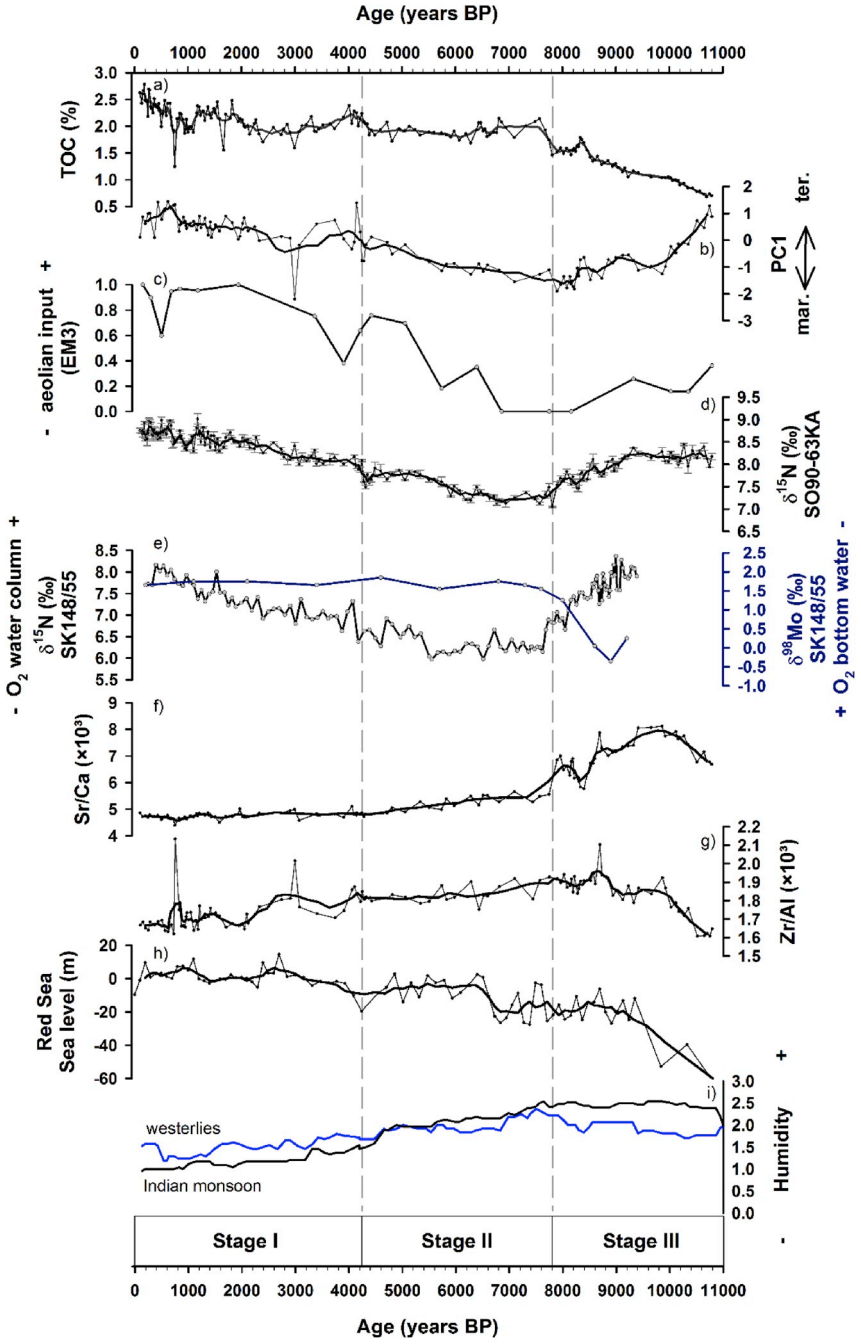

Fig. 7. Comparison of a) total organic carbon (TOC) and b) PC1 as indicator for marine vs. terrestrial input, c) EM3 indicating the aeolian input as well as d) $\delta^{15}N$, f) Sr/Ca and g) Zr/Al ratios of SO90-63 KA with e) $\delta^{15}N$ (black) and $\delta^{98}Mo$ (blue) of core SK148/55 (Kessarkar et al., 2018) h) sea level of the Red Sea (Siddall et al., 2003) and i) humidity index of the westerly and Indian monsoon region (Herzschuh, 2006). Thick black lines of TOC, PC1, $\delta^{15}N$, Sr/Ca, Zr/Al, and Red Sea sea level indicate five-point running average. (For interpretation of the references to colour in this figure legend, the reader is referred to the Web version of this article.)

needles from green algae and other biotic precipitates or with aragonite produced by pteropods which are best preserved under oxic conditions (Böning and Bard, 2009; Reichart et al., 1998, 1997). Pteropod shells are soluble under oxygen poor conditions (Klöcker and Henrich, 2006; Schulz et al., 1996; von Stackelberg, 1972), as these are associated with a low aragonite saturation state. For this reason, earlier studies linked variations in the Sr/Ca ratios to the aragonite compensation depth (ACD) so that higher Sr/Ca ratios in pelagic sediments were interpreted

Table 3
Comparison of $\delta^{13}C$ and $\delta^{18}O$ values of bulk carbonates (this study) and foraminifera (Staubwasser, 1999; Staubwasser et al., 2003) of SO90-63 KA with coccoliths from the tropical southern Atlantic (Fink et al., 2010) and regional soil carbonates from western India and Pakistan (Cerling and Quade, 1993; Laskar et al., 2013).

	Bulk carbonate sediments	Bulk carbonate C-layers	Planktic foraminifera	Coccoliths	Soil carbonates
$\delta^{13}C$ (‰ VPDB)	−0.81 ± 0.42	−1.32 ± 0.52	0.89 ± 0.15	0.13 ± 0.80	−3–−8
$\delta^{18}O$ (‰ VPDB)	−3.28 ± 0.71	−4.83 ± 1.30	−1.92 ± 0.15	−0.77 ± 0.91	−1–−5

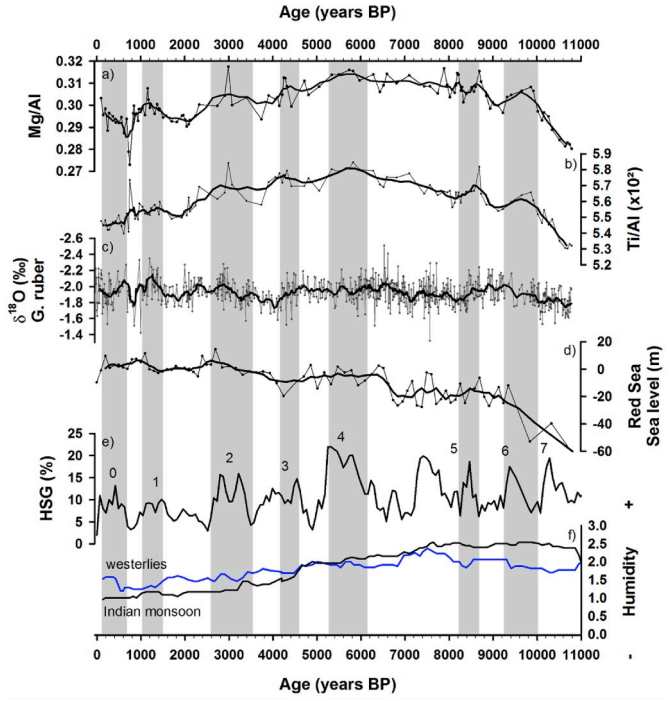

Fig. 8. Comparison of a) Mg/Al, b) Ti/Al ratios (this study) and c) *Globigerinoides ruber* $\delta^{18}O$ (Staubwasser et al., 2003) of SO90-63 KA with d) sea level of the Red Sea (Siddall et al., 2003), e) stacked North Atlantic hematite stained grains (HSG) as drift ice record from core MC52-V29191 (Bond et al., 2001) and e) humidity index of the westerly and Indian monsoon region (Herzschuh, 2006). Thick black lines of Mg/Al, Ti/Al and Red Sea sea level indicate five-point running average. Thick black line of $\delta^{18}O$ indicates 210 year moving average. Grey bars indicate Bond events (numbers) based on the HSG record by Bond et al. (2001). (For interpretation of the references to colour in this figure legend, the reader is referred to the Web version of this article.)

to indicate a deepening of the ACD. (Reichart et al., 1998, 1997). Studies found a correlation between aragonite and Sr/Ca suggested that varying aragonite content reflected OMZ intensity variations (Böning and Bard, 2009; Reichart et al., 1998), and that variations of aragonite supply play a minor role compared to OMZ intensity variations in controlling aragonite abundance (Böning and Bard, 2009). Following this argument means that high Sr/Ca ratios and low TOC concentrations in our core reflect a weaker OMZ during the early Holocene stage III, caused by lower sea level and/or better ventilated water masses in this region (Gaye et al., 2018). But as sediment redistribution also have affected sediment composition in the study area (Staubwasser and Sirocko, 2001; von Rad et al., 2002, 1995) Sr/Ca as oxygen indicator alone may yields ambiguous results. Therefore, additional parameters for the state of oxygenation are of advantage. The high Sr/Ca ratios during the early Holocene stage III is corroborated by the occurrence of *in situ* mollusc shells and low accumulation of authigenic U in the same part of the core, both indicating oxic conditions (Staubwasser and Dulski, 2002). In contrast, high $\delta^{15}N$ values between 10.8 and 8.8 ka BP indicates strong denitrification that argues against a weak OMZ. The $\delta^{15}N$ is often used as water column denitrification indicator in the Arabian Sea, with high (low) $\delta^{15}N$ values indicating more (less) denitrification due to suboxic conditions (e.g. Altabet et al., 1995; Gaye et al., 2013; Suthhof et al., 2001). The $\delta^{15}N$ values of modern surface sediments from the Indus margin have shown no clear cross-OMZ trend and are attributed to pelagic denitrification (Cowie et al., 2009). Further, it was found that there is no distinct relationship between $\delta^{15}N$ and bottom water oxygen on the Makran shelf and slope (Suthhof et al., 2001) and that, apart from O_2 concentration, hydrodynamic processes may play an important role for organic matter contribution across the OMZ (Cowie et al., 2014). However, reconstructions from SK148/55 within the OMZ offshore western India suggested that the bottom water was more oxygenated (indicated by lower $\delta^{98}Mo$ values) than the water column (indicated by higher $\delta^{15}N$ values) from 9.5 to 8.5 ka BP (Fig. 7e, Kessarkar et al., 2018). More oxic bottom water is consistent with the combination of high Sr/Ca, low TOC content and accumulation of authigenic U as well as absence of lamination, and occurrence of *in situ* mollusc shells in core SO90-63 KA. Whereas at the same time less oxygenated column waters leads to high $\delta^{15}N$ values. Between 8.8 and 7.8 ka BP low $\delta^{15}N$ values accompanied by high TOC contents and low Sr/Ca ratios (Fig. 7) indicate better oxygenation of the intermediate water column and more anoxic bottom water conditions on the Pakistan margin in line with conditions offshore western India (Kessarkar et al., 2018). This coincided with rising sea level and Kessarkar et al. (2018) attributed changes in O_2 bottom and intermediate water column conditions to reorganisation of subsurface water mass circulation. .

Several studies (Ansari and Vink, 2007; Enzel et al., 1999; Hamzeh et al., 2016a, 2016b; Wasson et al., 1984) suggest additional contribution of westerly associated precipitation to the likewise increased total annual and ISM dominated precipitation in the northwestern region dominated during the beginning of stage II (7–8 ka BP). The additional winter precipitation likely fed rivers and enhanced riverine transport of terrestrial material to the northeastern AS. Strengthening of ISM and additional precipitation by the westerlies increased fluvial input as suggested by the increase of EM1 and EM2 compared to EM3 at around 8 ka BP (Suppl. Fig. A5). In addition to EM3, the Mg/Al and Ti/Al ratios discriminate between aeolian and fluvial input. Ti is enriched in terrestrial detritus and is transported mainly by rivers to the Arabian Sea (Lückge et al., 2012, 2001). Dust from the Arabian peninsula, enriched in Mg, is transported by northwesterly winds from the Arabian desert and the Persian Gulf to the Makran continental slope (Deplazes et al., 2014; Prins et al., 2000; Sirocko et al., 2000, 1991; Sirocko and Lange, 1991). Dust from the Sistan region is enriched in Mg and has higher Mg/Al ratios (0.9 ± 0.16) compared to SO90-63 KA and, therefore, acts as possible aeolian source (Rashki, 2012). Both Mg/Al and Ti/Al display a similar pattern in our record. Highest Mg/Al ratios around ca. 5.5 to 6 ka BP suggest highest aeolian dust input during this period, which seems to contradict the implication of EM3 and the Ti/Al ratios. Model simulations suggest stronger northwesterly winds over the Sistan Basin as well as higher precipitation in the northwestern Himalayas during the mid-Holocene (ca. 6 ka BP) than today (Bush, 2002). The coincidence of strong westerly winds and high monsoon precipitation probably led to the observed synchronous pattern of aeolian and fluvial input. A decrease of the Indian monsoon humidity after 5 ka BP led to aridification along the Indus valley (Herzschuh, 2006; Ivory and Lézine, 2009) and a decrease in flood intensity of the Indus River (Giosan et al., 2012). Aridification likely occurred in other nearby regions of Pakistan, which is suggested by an increase of aeolian input (EM3) as well as a decrease of fluvial input (Ti/Al ratio) at ca. 5 ka BP recorded in SO90-63 KA. This is in line with results from the nearby core SO130-275 KL suggesting drier condition lasting from ca. 4 to 5 ka BP (Forke et al., 2019). Further evidence for a drier period during the mid-Holocene comes from palaeoreconstructions of Lake Hamoun in the Sistan Basin, which is at present dominated by winter precipitation (Hamzeh et al., 2016a, 2016b). During stage II the southward retreat of the ISM and enhanced westerlies in combination with the drier period in the Sistan region (Hamzeh et al., 2016a, 2016b) caused severe and frequent dust storms, which are the source of enhanced aeolian dust input suggested in our record at that time. Further, the enhanced westerlies and IWM in combination with higher sea level and reduced ventilation led to an intensification of the OMZ throughout the mid-Holocene (Gaye et al., 2018) mirrored by lower Sr/Ca ratios and increasing denitrification (higher $\delta^{15}N$ values) in our record (Fig. 7) as well as by increasing $\delta^{98}Mo$ and $\delta^{15}N$ values in SK148/55 (Kessarkar et al., 2018).

The dry spell around ca. 3.8–4.4 ka BP in the same record (Fig. 8, Staubwasser et al., 2003) and in many regional terrestrial records (e.g.

Menzel et al., 2014; Rawat et al., 2015), is identified in our record by enhanced aeolian input (EM3, Zr/Al) as well as the highest contribution of terrestrial material (PC1). It marks the transition between stage II and stage I. The properties are consistent with strong winds during this period and enhanced supply of dust probably derived from the Sistan region. The inferred aeolian intensification was also found in a pollen record of the nearby sediment core SO90-56 KA (Ivory and Lézine, 2009). They found high pollen input originating from the Baluchistan plateau, but less pollen associated either with long-distance riverine transport via the Indus River, or to summer and winter precipitation events.

The late Holocene (stage I) is characterized by higher terrestrial input (PC1) dominated by aeolian (EM3, Ti/Al) input and a gradual strengthening of OMZ conditions indicated by increasing $\delta^{15}N$. However, in contrast to the mid-Holocene phase (stage II), short-term variations are expressed during the late Holocene (stage I). A short phase of high marine input as well as an input of coarser terrestrial material is indicated between 2.9 and 3.1 ka BP. The attribution to marine or terrestrial sources is somewhat ambiguous, because Mg/Al imply increased aeolian, and Ti/Al implicate enhanced fluvial input. The peak Mg/Al ratio may originate from a dolomitic weathering source (Limmer et al., 2012) transported by high energy fluvial runoff, e.g., during a flood event. Giosan et al. (2012) reported relatively high fluvial activity of the Indus River system until 2.9 ka BP and pollen analyses indicate a weakening of winter monsoon wind strength since 3 ka BP (Ivory and Lézine, 2009). EM3 and elemental ratios (Zr/Al, Ti/Al) indicate highest aeolian input at ca. 2 ka BP (Roman Warm Period, RWP) and corroborate suggestions of an arid phase on the adjacent continent and a weak winter monsoon at this time period (Böll et al., 2014; Ivory and Lézine, 2009). Further to the west, southern Iran experienced dry conditions during the Medieval Warm Period (MWP, ca. 0.95–0.7 ka BP) and wet conditions during the Little Ice Age (LIA, ca. 0.65–0.1 ka BP) (Miller et al., 2016). The authors linked this to meridional shifts of the ITCZ, with a northward (southward) shift inducing drying (humidification) during warm (cold) periods. The antiphase behaviour of high ISM intensity and dry conditions along the Makran coast during warmer climate induce high fluvial input via the Pakistan rivers, but also high aeolian input from the Sistan and Makran region. This might explain the seeming contradiction of high fluvial and aeolian input during the RWP and MWP, and the synchronous decrease of both input sources during the LIA in our record.

In summary, sedimentation processes in the northeastern Arabian Sea during the early Holocene were affected primarily by the Indian Monsoon with gradual increase of the westerlies towards the late Holocene. Enhanced precipitation in the combined ISM and westerly realms resulted in higher fluvial input, whereas regional aridification and stronger westerly/winter monsoon winds favoured aeolian input from the adjacent Asian continent and particularly the Sistan Basin.

4.3. Other driving mechanisms of Holocene sedimentation process changes

Superposed on the long-term climatic drivers on the sedimentation processes (stage I – III) over the Holocene are short term variations/cycles. To detect such short term variations/cycles and to attribute them to putative drivers, we conducted spectral analyses on the time series of TOC, $CaCO_3$, $\delta^{15}N$, Mg/Al, Sr/Ca, Ti/Al, Zr/Al and PC1 of the SO90-63 KA sediments using the REDFIT3.8e MATLAB script (Schulz and Mudelsee, 2002). The spectral analysis displayed in Fig. 9 and Suppl. Fig. A6 identified periodicities of 1527 and 1425 years at significant levels (χ^2 > 90%) for Mg/Al and Ti/Al (Fig. 9). A further significant periodicity of 271–274 years is present in Mg/Al, Zr/Al and PC1 time series. The 1527 and 1425 year cycles are similar to those of the Holocene ice rafting-events, also known as Bond events (Bond et al., 2001, 1999, 1997), in the North Atlantic (Fig. 8). The Bond events 1, 2, 3, 4 and 6 coincide with high Mg/Al and Ti/Al ratios in the NE Arabian Sea record and also Bond event 0 (LIA) is marked by high Mg/Al ratios.

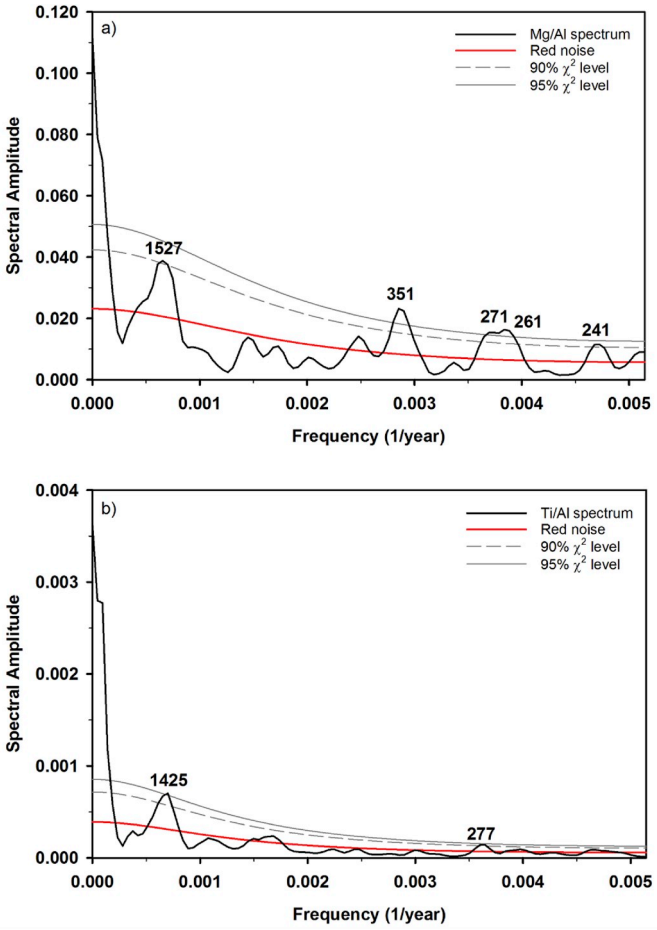

Fig. 9. Spectral analyses of a) Mg/Al and b) Ti/Al ratios of SO90-63 KA with red noise level (red line) as well as 90% χ^2- (dashed grey line) and 95% χ^2-level (grey line), respectively. (For interpretation of the references to colour in this figure legend, the reader is referred to the Web version of this article.)

The most pronounced event in SO90-63 KA is Bond event 2 at around 3 ka BP, characterized by high Mg/Al, Ti/Al and Zr/Al ratios, high $CaCO_3$ concentrations and low PC1 values (Figs. 7 and 8). Other regional records suggested a shift of moisture source and a change in moisture budget at this time. For instance, a multiproxy investigation of nearby core 56 KA indicates maximum precipitation and enhanced IWM activity at around 3.1 ka BP and the onset of gradual aridification at around 3 ka BP (Ivory and Lézine, 2009; Lückge et al., 2001). These authors postulated that the underlying reason were shifts in the ITCZ to a more southerly position during colder stages and a more northerly position during warmer stages. Previously, von Rad et al., 2002 described varve thickness variabilities and turbidite frequencies with a cyclicity of about 1470 years in northeastern AS sediments. Bond events are also associated with colder periods and weakened ISM in records of the Indian Monsoon realm (Bhushan et al., 2018; Das et al., 2017; Gupta et al., 2003; Munz et al., 2015; Rawat et al., 2015; Wanner et al., 2011).

The significant periodicity of 271–274 years is congruent with solar and/or tidal forcing. These periodicities are also found in other archives in this region, such as the Lonar Lake (274 years) (Menzel et al., 2014) and in the sediment core SO90-56 KA from the northeastern AS (250 and 280 years) (Berger and von Rad, 2002; von Rad et al., 1999a). Menzel et al. (2014) critically discussed the possibility of a solar cycle behind the prominent 274 year cycle in Lonar Lake sediment. In contrast, Berger and von Rad (2002) attributed the 280 year cycle in SO90-56 KA to a multiple of the 18.6 year Saros cycle, a lunar nodal tidal cycle. In additional to these periodicities the time series of $CaCO_3$, $\delta^{15}N$,

Mg/Al, Sr/Ca and TOC in the present record have significant periodicities on 121–126, 208–214, 253–261 and 351–358 years (Sup. Fig. A5). Similar periodicities have been reported earlier for other regional archives (Das et al., 2017; Duan et al., 2014; Fleitmann et al., 2003; Gupta et al., 2005; Menzel et al., 2014; Thamban et al., 2007; Wang et al., 2005), and have been attributed to distinct solar cycles, such as the de Vries cycle (~200–210 years) or the Hale cycle (~132 years).

But most prominent variations in our record, as in other regional records, can be linked to the Bond cycles suggesting a global (northern hemisphere) mechanism that drives short-term shifts of the Indian Monsoon and westerlies system. The shorter periods are consistent with impact of solar forcing and lunar nodal cycles that may have an impact on variations of the Indian Monsoon and westerlies system encoded in sediment records of the northeastern AS.

5. Conclusions

The geochemical analyses of the high-resolution sediment record SO90-63 KA reveal changes in sedimentation processes and their driving mechanism in the northeastern AS over the Holocene. The northeastern AS is a critical region influenced by the interaction of the Indian Monsoon and the westerly realm. The Hab River is the main contributor of fluvial sediments, dust from the Sistan region as well as other deserts on the adjacent Asian continent is a more important sediment source than dust from the Arabian Peninsula. The elemental composition and carbonate isotope analyses of the C-event layers, which are also prominent in other cores from the northeastern AS, indicate a fluvial origin and deposition under high transport energy.

The sedimentation pattern in the northeastern Arabian Sea recorded in SO90-63 KA evolved in three main stages:

Stage III (10.8 – ca. 7.8 ka BP, early Holocene): This stage was characterized by a transition from a predominantly terrestrial towards a marine dominated sedimentation due to the post-glacial sea level rise and the orbitally forced strengthening of the ISM. At the beginning of stage III discharges predominantly of the Hab and other rivers along the Makran coast controlled the sedimentation at our study site and association with high productivity and a weak OMZ. During sea level rise between 10.8 ka and ca. 8.2 ka BP sedimentation pattern changed. The retreating coast line weakened the influence of the Makran rivers, whereas the strengthening of the ISW in association with enhanced westerly induced winter precipitation increased inputs from the Hab River. However, overall impacts of river discharges decreased and the intensification of the ISM and resulting enhanced productivity established a marine dominated sedimentation.

Stage II (ca. 7.8 – ca. 4.2 ka BP, mid-Holocene): This period is characterized by a transition from wet towards more arid conditions and increasing westerly influence. The southward retreat of the ITCZ, the decreasing ISM intensity and increasing IWM/westerly strength resulted in decreasing fluvial and increasing aeolian input. Further, enhanced IWM and westerlies as well as a reduced ventilation strengthened the OMZ in the northeastern Arabian Sea.

Stage I (ca. 4.2 ka BP – recent, late Holocene): The late Holocene saw a further weakening of the ISM and enhanced aridification in the catchment of the Hab River. This decreased river discharged and increased aeolian input, whereas the strengthening of the OMZ continued, which started during stage II.

These general trends are superposed by short term variations during the early (stage III) and also late Holocene (stage I), respectively. A marked increase of fluvial input occurred around 8.4–8.6 ka BP and at ca. 3 ka BP, whereas dry events are evident around 4.2 ka BP and 1–1.2 ka BP. Spectral analyses reveal pronounced frequencies of 1425–1527 years that correspond with Bond events found in the North Atlantic. Shorter significant periodicities (121, 208–214, 253–261, 271–274 and 351–355 years) identified in the spectral analyses correspond to solar and lunar nodal cycles. Our study documents that the influence of the westerlies became increasingly important throughout the Holocene. Further, our study stresses the importance of the interplay of the Indian Monsoon, the westerlies and solar and lunar driven short-term cycle on the sedimentation processes in the northeastern AS.

Acknowledgements

We thank F. Langenberg, M. Metzke, Y. Akkul, C. Staschok and H. Kuhnert for analytical support. A. Hahn and M. Kölling are thanked for the discussion on the elemental composition. We thank M. Staubwasser and two anonymous reviewers for their constructive and helpful comments to highly improve this manuscript. This study was funded by the German Federal Ministry of Education and Research (BMBF) as part of CAHOL (Central Asian Holocene Climate, project number 03G0864A), a subproject of the research programm CAME II (Central Asia: Climatic Tipping Points & Their Consequences, project number 03G0863G).

Appendix A. Supplementary data

Supplementary data to this article can be found online at https://doi.org/10.1016/j.dsr2.2019.03.003.

References

Ahmed, Z., 1993. Leucocratic rocks from the bela ophiolite, Khuzdar district, Pakistan. Geol. Soc. London, Spec. Publ. 74, 89–100. https://doi.org/10.1144/GSL.SP.1993.074.01.07.

Ahmed, Z., Ernst, W.G., 1999. Island arc–related, back-arc basinal, and oceanic-island components of the bela ophiolite-mélange complex, Pakistan. Int. Geol. Rev. 41, 739–763. https://doi.org/10.1080/00206819909465167.

Alam, K., Trautmann, T., Blaschke, T., 2011. Aerosol optical properties and radiative forcing over mega-city Karachi. Atmos. Res. 101, 773–782. https://doi.org/10.1016/j.atmosres.2011.05.007.

Alizai, A., Carter, A., Clift, P.D., VanLaningham, S., Williams, J.C., Kumar, R., 2011. Sediment provenance, reworking and transport processes in the Indus River by U–Pb dating of detrital zircon grains. Glob. Planet. Chang. 76, 33–55. https://doi.org/10.1016/j.gloplacha.2010.11.008.

Altabet, M.A., Francois, R., Murray, D.W., Prell, W.L., 1995. Climate-related variations in denitrification in the Arabian Sea from sediment 15N/14N ratios. Nature 373, 506–509. https://doi.org/10.1038/373506a0.

Andruleit, H.A., von Rad, U., Bruns, A., Ittekkot, V., 2000. Coccolithophore fluxes from sediment traps in the northeastern Arabian Sea off Pakistan. Mar. Micropaleontol. 38, 285–308.

Anoop, A., Prasad, S., Krishnan, R., Naumann, R., Dulski, P., 2013. Intensified monsoon and spatiotemporal changes in precipitation patterns in the NW Himalaya during the early-mid Holocene. Quat. Int. 313, 74–84. https://doi.org/10.1016/j.quaint.2013.08.014.

Ansari, M.H., Vink, A., 2007. Vegetation history and palaeoclimate of the past 30 kyr in Pakistan as inferred from the palynology of continental margin sediments off the Indus Delta. Rev. Palaeobot. Palynol. 145, 201–216. https://doi.org/10.1016/j.revpalbo.2006.10.005.

Berger, W.H., von Rad, U., 2002. Decadal to millennial cyclicity in varves and turbidites from the Arabian Sea: hypothesis of tidal origin. Glob. Planet. Chang. 34, 313–325. https://doi.org/10.1016/S0921-8181(02)00122-4.

Bhushan, R., Sati, S.P., Rana, N., Shukla, A.D., Mazumdar, A.S., Juyal, N., 2018. High-resolution millennial and centennial scale Holocene monsoon variability in the Higher Central Himalayas. Palaeogeogr. Palaeoclimatol. Palaeoecol. 489, 95–104. https://doi.org/10.1016/j.palaeo.2017.09.032.

Böll, A., Lückge, A., Munz, P., Forke, S., Schulz, H., Ramaswamy, V., Rixen, T., Gaye, B., Emeis, K.C., 2014. Late Holocene primary productivity and sea surface temperature variations in the northeastern Arabian Sea: implications for winter monsoon variability. Paleoceanography. https://doi.org/10.1002/2013PA002579.

Böll, A., Schulz, H., Munz, P., Rixen, T., Gaye, B., Emeis, K.C., 2015. Contrasting sea surface temperature of summer and winter monsoon variability in the northern Arabian Sea over the last 25ka. Palaeogeogr. Palaeoclimatol. Palaeoecol. 426, 10–21. https://doi.org/10.1016/j.palaeo.2015.02.036.

Bond, G., Kromer, B., Beer, J., Muscheler, R., Evans, M.N., Showers, W., Hoffmann, S., Lotti-Bond, R., Hajdas, I., Bonani, G., 2001. Persistent solar influence on North Atlantic climate during the holocene. Science 294, 2130–2136. https://doi.org/10.1126/science.1065680.

Bond, G., Showers, W., Cheseby, M., Lotti, R., Almasi, P., deMenocal, P., Priore, P., Cullen, H., Hajdas, I., Bonani, G., 1997. A pervasive millennial-scale cycle in north atlantic holocene and glacial climates. Science 278 (80), 1257–1266. https://doi.org/10.1126/science.278.5341.1257.

Bond, G., Showers, W., Elliot, M., Evans, M., Lotti, R., Hajdas, I., Bonani, G., Johnson, S., 1999. the North atlantic's 1-2 kyr climate rhythm: relation to heinrich events, dansgaard/oeschger cycles and the Little ice age. Mech. Glob. Clim. Chang. Millenn. time scales, Geophys. Monogr. 112, 35–58. https://doi.org/10.1029/GM112p0035.

Böning, P., Bard, E., 2009. Millennial/centennial-scale thermocline ventilation changes in the Indian Ocean as reflected by aragonite preservation and geochemical variations

in Arabian Sea sediments. Geochim. Cosmochim. Acta 73, 6771–6788. https://doi.org/10.1016/j.gca.2009.08.028.
Bookhagen, B., Burbank, D.W., 2010. Toward a complete Himalayan hydrological budget: spatiotemporal distribution of snowmelt and rainfall and their impact on river discharge. J. Geophys. Res. Earth Surf 115. https://doi.org/10.1029/2009JF001426.
Bourget, J., Zaragosi, S., Ellouz-Zimmermann, N., Mouchot, N., Garlan, T., Schneider, J.L., Lanfumey, V., Lallemant, S., 2011. Turbidite system architecture and sedimentary processes along topographically complex slopes: the Makran convergent margin. Sedimentology 58, 376–406. https://doi.org/10.1111/j.1365-3091.2010.01168.x.
Bourget, J., Zaragosi, S., Ellouz-Zimmermann, S., Ducassou, E., Prins, M.A., Garlan, T., Lanfumey, V., Schneider, J.L., Rouillard, P., Giraudeau, J., 2010. Highstand vs. lowstand turbidite system growth in the Makran active margin: imprints of high-frequency external controls on sediment delivery mechanisms to deep water systems. Mar. Geol. 274, 187–208. https://doi.org/10.1016/j.margeo.2010.04.005.
Bourget, J., Zaragosi, S., Rodriguez, M., Fournier, M., Garlan, T., Chamot-Rooke, N., 2013. Late quaternary megaturbidites of the indus fan: origin and stratigraphic significance. Mar. Geol. 336, 10–23. https://doi.org/10.1016/j.margeo.2012.11.011.
Bush, A.B.G., 2002. A comparison of simulated monsoon circulations and snow accumulation in Asia during the mid-Holocene and at the Last Glacial Maximum. Glob. Planet. Chang. 32, 331–347. https://doi.org/10.1016/S0921-8181(02)00074-7.
Caley, T., Malaizé, B., Zaragosi, S., Rossignol, L., Bourget, J., Eynaud, F., Martinez, P., Giraudeau, J., Charlier, K., Ellouz-Zimmermann, N., 2011. New Arabian Sea records help decipher orbital timing of Indo-Asian monsoon. Earth Planet. Sci. Lett. 308, 433–444. https://doi.org/10.1016/j.epsl.2011.06.019.
Cerling, T.E., Quade, J., 1993. Stable carbon and oxygen isotopes in soil carbonates. Clim. Chang. Cont. Isot. Rec. 217–231. https://doi.org/10.1029/GM078p0217.
Chauhan, O.S., Jayakumar, S., Menezes, A.A.A., Rajawat, A.S., Nayak, S.R., 2006. Anomalous inland influx of the river indus, Gulf of Kachchh, India. Mar. Geol. 229, 91–100. https://doi.org/10.1016/j.margeo.2005.12.003.
Clift, P.D., Giosan, L., Blusztajn, J., Campbell, I.H., Allen, C., Pringle, M., Tabrez, A.R., Danish, M., Rabbani, M.M., Alizai, A., Carter, A., Lückge, A., 2008. Holocene erosion of the Lesser Himalaya triggered by intensified summer monsoon. Geology 36, 79–82. https://doi.org/10.1130/G24315A.1.
Cowie, G., Mowbray, S., Kurian, S., Sarkar, A., White, C., Anderson, A., Vergnaud, B., Johnstone, G., Brear, S., Woulds, C., Naqvi, S.W.A., Kitazato, H., 2014. Comparative organic geochemistry of Indian margin (Arabian Sea) sediments: estuary to continental slope. Biogeosciences 11, 6683–6696. https://doi.org/10.5194/bg-11-6683-2014.
Cowie, G.L., Mowbray, S., Lewis, M., Matheson, H., McKenzie, R., 2009. Carbon and nitrogen elemental and stable isotopic compositions of surficial sediments from the Pakistan margin of the Arabian Sea. Deep. Res. Part II Top. Stud. Oceanogr. 56, 271–282. https://doi.org/10.1016/j.dsr2.2008.05.031.
Das, M., Singh, R.K., Gupta, A.K., Bhaumik, A.K., 2017. Holocene strengthening of the Oxygen Minimum Zone in the northwestern Arabian Sea linked to changes in intermediate water circulation or Indian monsoon intensity? Palaeogeogr. Palaeoclimatol. Palaeoecol. 483, 125–135. https://doi.org/10.1016/j.palaeo.2016.10.035.
Demske, D., Tarasov, P.E., Wünnemann, B., Riedel, F., 2009. Late glacial and Holocene vegetation, Indian monsoon and westerly circulation in the Trans-Himalaya recorded in the lacustrine pollen sequence from Tso Kar, Ladakh, NW India. Palaeogeogr. Palaeoclimatol. Palaeoecol. 279, 172–185. https://doi.org/10.1016/j.palaeo.2009.05.008.
Deplazes, G., Lückge, A., Stuut, J.B.W., Pätzold, J., Kuhlmann, H., Husson, D., Fant, M., Haug, G.H., 2014. Weakening and strengthening of the Indian monsoon during Heinrich events and Dansgaard-Oeschger oscillations. Paleoceanography 29, 99–114. https://doi.org/10.1002/2013PA002509.
Dietze, E., Hartmann, K., Diekmann, B., IJmker, J., Lehmkuhl, F., Opitz, S., Stauch, G., Wünnemann, B., Borchers, A., 2012. An end-member algorithm for deciphering modern detrital processes from lake sediments of Lake Donggi Cona, NE Tibetan Plateau, China. Sediment. Geol. 243, 169–180. https://doi.org/10.1016/j.sedgeo.2011.09.014.
Dixit, Y., Hodell, D.A., Sinha, R., Petrie, C.A., 2014. Abrupt weakening of the Indian summer monsoon at 8.2 kyr B.P. Earth Planet. Sci. Lett. 391, 16–23. https://doi.org/10.1016/j.epsl.2014.01.026.
Duan, F., Wang, Y., Shen, C.C., Wang, Y., Cheng, H., Wu, C.C., Hu, H.M., Kong, X., Liu, D., Zhao, K., 2014. Evidence for solar cycles in a late Holocene speleothem record from dongge cave, China. Sci. Rep. 4, 1–7. https://doi.org/10.1038/srep05159.
Dypvik, H., Harris, N.B., 2001. Geochemical facies analysis of fine-grained siliciclastics using Th/U, Zr/Rb and (Zr+Rb)/Sr ratios. Chem. Geol. 181, 131–146. https://doi.org/10.1016/S0009-2541(01)00278-9.
Enzel, Y., Ely, L.L., Mishra, R., Ramesh, R., Amit, R., Lazar, B., Rajaguru, S.N., Baker, V.R., Sandler, A., 1999. High-resolution holocene environmental changes in the thar desert, northwestern India. Science 284, 125–128. https://doi.org/10.1126/science.284.5411.125. (80-.).
Fink, C., Baumann, K.-H., Groeneveld, J., Steinke, S., 2010. Strontium/Calcium ratio, carbon and oxygen stable isotopes in coccolith carbonate from different grain-size fractions in South Atlantic surface sediments. Geobios 43, 151–164. https://doi.org/10.1016/j.geobios.2009.11.001.
Fleitmann, D., Burns, S.J., Mangini, A., Mudelsee, M., Kramers, J., Villa, I., Neff, U., Al-Subbary, A.A., Buettner, A., Hippler, D., Matter, A., 2007. Holocene ITCZ and Indian monsoon dynamics recorded in stalagmites from Oman and Yemen (Socotra). Quat. Sci. Rev. 26, 170–188. https://doi.org/10.1016/j.quascirev.2006.04.012.
Fleitmann, D., Burns, S.J., Mudelsee, M., Neff, U., Kramers, J., Mangini, A., Matter, A., 2003. Holocene forcing of the Indian monsoon recorded in a stalagmite from southern Oman. Science 300 (80), 1737–1739.
Forke, S., Rixen, T., Burdanowitz, N., Ramaswamy, V., Munz, P., Wilhelms-dick, D., Vogt, C., Kasten, S., Gaye, B., 2019. Sources of laminated sediments in the northeastern Arabian Sea off Pakistan and implications for sediment transport mechanisms during the late Holocene. The Holocene 29, 130–144. https://doi.org/10.1177/0959683618804627.
Fralick, P.W., Kronberg, B.I., 1997. Geochemical discrimination of clastic sedimentary rock sources. Sediment. Geol. 113, 111–124. https://doi.org/10.1016/S0037-0738(97)00049-3.
Gaye, B., Böll, A., Segschneider, J., Burdanowitz, N., Emeis, K.-C., Ramaswamy, V., Lahajnar, N., Lückge, A., Rixen, T., 2018. Glacial–interglacial changes and holocene variations in Arabian Sea denitrification. Biogeosciences 15, 507–527. https://doi.org/10.5194/bg-15-507-2018.
Gaye, B., Nagel, B., Dähnke, K., Rixen, T., Emeis, K.C., 2013. Evidence of parallel denitrification and nitrite oxidation in the ODZ of the Arabian Sea from paired stable isotopes of nitrate and nitrite. Glob. Biogeochem. Cycles 27, 1059–1071. https://doi.org/10.1002/2011GB004115.
Giosan, L., Clift, P.D., Macklin, M.G., Fuller, D.Q., Constantinescu, S., Durcan, J.A., Stevens, T., Duller, G.A.T., Tabrez, A.R., Gangal, K., Adhikari, R., Alizai, A., Filip, F., VanLaningham, S., Syvitski, J.P.M., 2012. Fluvial landscapes of the Harappan civilization. Proc. Natl. Acad. Sci. U.S.A. 109, E1688–E1694. https://doi.org/10.1073/pnas.1112743109.
Gupta, A.A.K., Anderson, D.D.M., Overpeck, J.J.T., 2003. Abrupt changes in the asian southwest monsoon during the holocene and their links to the north Atlantic Ocean. Nature 421, 354–357. https://doi.org/10.1038/nature01340.
Gupta, A.K., Das, M., Anderson, D.M., 2005. Solar influence on the Indian summer monsoon during the Holocene. Geophys. Res. Lett. 32, 2–5. https://doi.org/10.1029/2005GL022685.
Hamzeh, M.A., Gharaie, M.H.M., Lahijani, H.A.K., Djamali, M., Harami, R.M., Beni, A.N., 2016a. Holocene hydrological changes in SE Iran, a key region between Indian Summer Monsoon and Mediterranean winter precipitation zones, as revealed from a lacustrine sequence from Lake Hamoun. Quat. Int. 408, 25–39. https://doi.org/10.1016/j.quaint.2015.11.011.
Hamzeh, M.A., Mahmudy-gharaie, M.H., Alizadeh-lahijani, H., Moussavi-harami, R., Djamali, M., Naderi-beni, A., 2016b. Paleolimnology of Lake Hamoun (E Iran): implication for past climate changes and possible impacts on human settlements. Palaios 31, 616–629. https://doi.org/10.2110/palo.2016.055.
Hashimi, N.H., Nigam, R., Nair, R.R., Rajagopalan, G., 1995. Holocene Sea Level Fluctuations on Western Indian Continental Margin: an Update.
Herzschuh, U., 2006. Palaeo-moisture evolution in monsoonal Central Asia during the last 50,000 years. Quat. Sci. Rev. 25, 163–178. https://doi.org/10.1016/j.quascirev.2005.02.006.
Holben, B.N., Eck, T.F., Slutsker, I., Tanré, D., Buis, J.P., Setzer, A., Vermote, E., Reagan, J.A., Kaufman, Y.J., Nakajima, T., Lavenu, F., Jankowiak, I., Smirnov, A., 1998. AERONET—a federated instrument Network and data archive for aerosol characterization. Remote Sens. Environ. 66, 1–16. https://doi.org/10.1016/S0034-4257(98)00031-5.
Holben, B.N., Tanré, D., Smirnov, A., Eck, T.F., Slutsker, I., Abuhassan, N., Newcomb, W.W., Schafer, J.S., Chatenet, B., Lavenu, F., Kaufman, Y.J., Castle, J. Vande, Setzer, A., Markham, B., Clark, D., Frouin, R., Halthore, R., Karneli, A., O'Neill, N.T., Pietras, C., Pinker, R.T., Voss, K., Zibordi, G., 2001. An emerging ground-based aerosol climatology: aerosol optical depth from AERONET. J. Geophys. Res. Atmos. 106, 12067–12097. https://doi.org/10.1029/2001JD900014.
Hussain, B.A., Mir, H., Afzal, M., 2005. Analysis of dust storms frequency over Pakistan during 1961-2000. Pakisan J. Meteorol. 2.
Ivory, S.J., Lézine, A.M., 2009. Climate and environmental change at the end of the Holocene Humid Period: a pollen record off Pakistan. Compt. Rendus Geosci. 341, 760–769. https://doi.org/10.1016/j.crte.2008.12.009.
Karim, A., Veizer, J., 2002. Water balance of the Indus River Basin and moisture source in the Karakoram and western Himalayas: implications from hydrogen and oxygen isotopes in river water. J. Geophys. Res. Atmos. 107https://doi.org/10.1029/2000JD000253. ACH 9-1-ACH 9-12.
Kaskaoutis, D.G., Rashki, A., Francois, P., Dumka, U.C., Houssos, E.E., Legrand, M., 2015a. Meteorological regimes modulating dust outbreaks in southwest Asia: the role of pressure anomaly and Inter-Tropical Convergence Zone on the 1–3 July 2014 case. Aeolian Res 18, 83–97. https://doi.org/10.1016/j.aeolia.2015.06.006.
Kaskaoutis, D.G., Rashki, A., Houssos, E.E., Goto, D., Nastos, P.T., 2014. Extremely high aerosol loading over Arabian Sea during June 2008: the specific role of the atmospheric dynamics and Sistan dust storms. Atmos. Environ. 94, 374–384. https://doi.org/10.1016/j.atmosenv.2014.05.012.
Kaskaoutis, D.G., Rashki, A., Houssos, E.E., Mofidi, A., Goto, D., Bartzokas, A., Francois, P., Legrand, M., 2015b. Meteorological aspects associated with dust storms in the Sistan region, southeastern Iran. Clim. Dyn. 45, 407–424. https://doi.org/10.1007/s00382-014-2208-3.
Kessarkar, P.M., Naqvi, S.W.A., Thamban, M., Fernandes, L.L., Siebert, C., Rao, V.P., Kawahata, H., Ittekkot, V., Frank, M., 2018. Variations in denitrification and ventilation within the Arabian Sea oxygen minimum zone during the holocene. Geochem. Geophys. Geosyst. 19, 2179–2193. https://doi.org/10.1029/2017GC007286.
Klöcker, R., Henrich, R., 2006. Recent and Late Quaternary pteropod preservation on the Pakistan shelf and continental slope. Mar. Geol. 231, 103–111. https://doi.org/10.1016/j.margeo.2006.05.014.
Kolla, V., Kostecki, J.A., Robinson, F., Biscaye, P.E., Ray, P.K., 1981. Distributions and origins of clay minerals and quartz in surface sediments of the Arabian Sea. J. Sediment. Res. 51, 563–569.
Laskar, a., Yadava, M., Sharma, N., Ramesh, R., 2013. Late-Holocene climate in the Lower Narmada valley, Gujarat, western India, inferred using sedimentary carbon and oxygen isotope ratios. Holocene 23, 1115–1122. https://doi.org/10.1177/0959683613483621.
Limmer, D.R., Bning, P., Giosan, L., Ponton, C., Köhler, C.M., Cooper, M.J., Tabrez, A.R.,

Clift, P.D., 2012. Geochemical record of holocene to recent sedimentation on the western indus continental shelf, Arabian Sea. Geochem. Geophys. Geosyst. 13, 1–27. https://doi.org/10.1029/2011GC003845.
Lückge, A., Deplazes, G., Schulz, H., Scheeder, G., Suckow, A., Kasten, S., Haug, G.H., 2012. Impact of indus River discharge on productivity and preservation of organic carbon in the Arabian Sea over the Twentieth century. Geology 40, 399–402. https://doi.org/10.1130/G32608.1.
Lückge, A., Doose-Rolinski, H., Khan, A., Schulz, H., von Rad, U., 2001. Monsoonal variability in the northeastern Arabian Sea during the past 5000 years: geochemical evidence from laminated sediments. Palaeogeogr. Palaeoclimatol. Palaeoecol. 167, 273–286. https://doi.org/10.1016/S0031-0182(00)00241-8.
Lückge, A., Reinhardt, L., Andruleit, H., Doose-Rolinski, H., von Rad, U., Schulz, H., Treppke, U., 2002. Formation of varve-like laminae off Pakistan: decoding 5 years of sedimentation. Geol. Soc. London, Spec. Publ. 195, 421–431. https://doi.org/10.1144/GSL.SP.2002.195.01.23.
Lutz, A.F., Immerzeel, W.W., Shrestha, A.B., Bierkens, M.F.P., 2014. Consistent increase in High Asia's runoff due to increasing glacier melt and precipitation. Nat. Clim. Change 4, 587–592. https://doi.org/10.1038/nclimate2237.
Mahowald, N., Albani, S., Kok, J.F., Engelstaeder, S., Scanza, R., Ward, D.S., Flanner, M.G., 2014. The size distribution of desert dust aerosols and its impact on the Earth system. Aeolian Res 15, 53–71. https://doi.org/10.1016/j.aeolia.2013.09.002.
Mahowald, N.M., Baker, A.R., Bergametti, G., Brooks, N., Duce, R.A., Jickells, T.D., Kubilay, N., Prospero, J.M., Tegen, I., 2005. Atmospheric global dust cycle and iron inputs to the ocean. Glob. Biogeochem. Cycles 19. https://doi.org/10.1029/2004GB002402.
McCave, I.N., 1972. Transport and escape of fine-grained sediment from shelf areas. Shelf Sediment Transp. Process. Pattern.
Menzel, P., Gaye, B., Mishra, P.K., Anoop, A., Basavaiah, N., Marwan, N., Plessen, B., Prasad, S., Riedel, N., Stebich, M., Wiesner, M.G., 2014. Linking holocene drying trends from Lonar lake in monsoonal central India to North Atlantic cooling events. Palaeogeogr. Palaeoclimatol. Palaeoecol. 410, 164–178. https://doi.org/10.1016/j.palaeo.2014.05.044.
Miller, C.S., Leroy, S.A.G., Collins, P.E.F., Lahijani, H.A.K., 2016. Late Holocene vegetation and ocean variability in the Gulf of Oman. Quat. Sci. Rev. 143, 120–132. https://doi.org/10.1016/j.quascirev.2016.05.010.
Munz, P.M., Lückge, A., Siccha, M., Böll, A., Forke, S., Kucera, M., Schulz, H., 2017. The Indian winter monsoon and its response to external forcing over the last two and a half centuries. Clim. Dyn. 49, 1801–1812. https://doi.org/10.1007/s00382-016-3403-1.
Munz, P.M., Siccha, M., Lückge, A., Böll, A., Kucera, M., Schulz, H., 2015. Decadal-resolution record of winter monsoon intensity over the last two millennia from planktic foraminiferal assemblages in the northeastern Arabian Sea. Holocene. https://doi.org/10.1177/0959683615591357.
Pease, P.P., Tchakerian, V.P., Tindale, N.W., 1998. Aerosols over the Arabian Sea: geochemistry and source areas for aeolian desert dust. J. Arid Environ. 39, 477–496. https://doi.org/10.1006/jare.1997.0368.
Prasad, S., Enzel, Y., 2006. Holocene paleoclimates of India. Quat. Res. 66, 442–453. https://doi.org/10.1016/j.yqres.2006.05.008.
Prins, M., Postma, G., Weltje, G., 2000. Controls on terrigenous sediment supply to the Arabian Sea during the late Quaternary: the Makran continental slope. Mar. Geol. 169, 351–371. https://doi.org/10.1016/S0025-3227(00)00087-6.
Rashki, A., 2012. Seasonality and Mineral, Chemical and Optical Properties of Dust Storms in the Sistan Region of Iran, and Their Influence on Human Health. University of Pretoria, South Africa.
Rashki, A., Arjmand, M., Kaskaoutis, D.G., 2017. Assessment of dust activity and dust-plume pathways over Jazmurian Basin, southeast Iran. Aeolian Res 24, 145–160. https://doi.org/10.1016/j.aeolia.2017.01.002.
Rashki, A., Eriksson, P.G., Rautenbach, C.J. d. W., Kaskaoutis, D.G., Grote, W., Dykstra, J., 2013. Assessment of chemical and mineralogical characteristics of airborne dust in the Sistan region, Iran. Chemosphere 90, 227–236. https://doi.org/10.1016/j.chemosphere.2012.06.059.
Rashki, A., Kaskaoutis, D.G., Francois, P., Kosmopoulos, P.G., Legrand, M., 2015. Dust-storm dynamics over Sistan region, Iran: seasonality, transport characteristics and affected areas. Aeolian Res 16, 35–48. https://doi.org/10.1016/j.aeolia.2014.10.003.
Rashki, A., Kaskaoutis, D.G., Rautenbach, C.J. deW., Eriksson, P.G., Qiang, M., Gupta, P., 2012. Dust storms and their horizontal dust loading in the Sistan region, Iran. Aeolian Res 5, 51–62. https://doi.org/10.1016/j.aeolia.2011.12.001.
Rawat, S., Gupta, A.K., Sangode, S.J., Srivastava, P., Nainwal, H.C., 2015. Late pleistocene–holocene vegetation and Indian summer monsoon record from the Lahaul, northwest himalaya, India. Quat. Sci. Rev. 114, 167–181. https://doi.org/10.1016/j.quascirev.2015.01.032.
Reichart, G.J., den Dulk, M., Visser, H.J., van der Weijden, C.H., Zachariasse, W.J., 1997. A 225 kyr record of dust supply, paleoproductivity and the oxygen minimum zone from the Murray Ridge (northern Arabian Sea). Palaeogeogr. Palaeoclimatol. Palaeoecol. 134, 149–169. https://doi.org/10.1016/S0031-0182(97)00071-0.
Reichart, G.J., Lourens, L.J., Zachariasse, W.J., 1998. Temporal variability in the northern Arabian Sea oxygen minimum zone (OMZ) during the last 225,000 years. Paleoceanography 13, 607–621. https://doi.org/10.1029/98PA02203.
Reichart, G.J., Nortier, J., Versteegh, G., Zachariasse, W.J., 2002. Periodical breakdown of the Arabian Sea oxygen minimum zone caused by deep convective mixing. Geol. Soc. London, Spec. Publ. 195, 407–419. https://doi.org/10.1144/GSL.SP.2002.195.01.22.
n.d.Resmi, M.R., Achyuthan, H., 2018. Northeast monsoon variations during the Holocene inferred from palaeochannels and active channels of the Palar River basin, Southern Peninsular India. Holocene 0https://doi.org/10.1177/0959683617752839.
959683617752839.
Saher, M.H., Peeters, F.J.C., Kroon, D., 2007. Sea surface temperatures during the SW and NE monsoon seasons in the western Arabian Sea over the past 20,000 years. Palaeogeogr. Palaeoclimatol. Palaeoecol. 249, 216–228. https://doi.org/10.1016/j.palaeo.2007.01.014.
Sarkar, A., Ramesh, R., Somayajulu, B.L.K., Agnihotri, R., Jull, A.J.T., Burr, O.S., 2000. High resolution Holocene monsoon record from the eastern Arabian Sea. Earth Planet. Sci. Lett. 177, 209–218. https://doi.org/10.1016/S0012-821X(00)00053-4.
Schott, W., von Stackelberg, U., Eckhardt, F.J., Mattiat, B., Peters, J., Zobel, B., 1970. Geologische Untersuchungen an Sedimenten des indisch-pakistanischen Kontinentalrandes (Arabisches Meer). Geol. Rundsch. 60, 264–275. https://doi.org/10.1007/BF01820944.
Schulz, H., von Rad, U., Ittekkot, V., 2002. Planktic foraminifera, particle flux and oceanic productivity off Pakistan, NE Arabian Sea: modern analogues and application to the palaeoclimatic record. Geol. Soc. London, Spec. Publ. 195, 499–516. https://doi.org/10.1144/GSL.SP.2002.195.01.27.
Schulz, H., Von Rad, U., Von Stackelberg, U., 1996. Laminated sediments from the oxygen-minimum zone of the northeastern Arabian Sea. Geol. Soc. London, Spec. Publ. 116, 185–207. https://doi.org/10.1144/GSL.SP.1996.116.01.16.
Schulz, M., Mudelsee, M., 2002. REDFIT: estimating red-noise spectra directly from unevenly spaced paleoclimatic time series. Comput. Geosci. 28, 421–426. https://doi.org/10.1016/S0098-3004(01)00044-9.
Shimmield, G.B., Mowbray, S.R., 1991. The inorganic geochemical record of the northwest Arabian Sea: a history of productivity variation over the last 400 K.Y. From sites 722 and 724. Proc. Ocean Drill. Progr. Sci. Results 117, 409–420.
Siddall, M., Rohling, E.J., Almogi-Labin, A., Hemleben, C., Meischner, D., Schmelzer, I., Smeed, D.A., 2003. Sea-level fluctuations during the last glacial cycle. Nature 423, 853–858.
Sinha, R., Smykatz-Kloss, W., Stüben, D., Harrison, S.P., Berner, Z., Kramar, U., 2006. Late Quaternary palaeoclimatic reconstruction from the lacustrine sediments of the Sambhar playa core, Thar Desert margin, India. Palaeogeogr. Palaeoclimatol. Palaeoecol. 233, 252–270. https://doi.org/10.1016/j.palaeo.2005.09.012.
Sirocko, F., Garbe-Schönberg, D., Devey, C., 2000. Processes controlling trace element geochemistry of Arabian Sea sediments during the last 25,000 years. Glob. Planet. Chang. 26, 217–303. https://doi.org/10.1016/S0921-8181(00)00046-1.
Sirocko, F., Lange, H., 1991. Clay-mineral accumulation rates in the Arabian Sea during the late quaternary. Mar. Geol. 97, 105–119. https://doi.org/10.1016/0025-3227(91)90021-U.
Sirocko, F., Sarnthein, M., Lange, H., Erlenkeuser, H., 1991. Atmospheric summer circulation and coastal upwelling in the Arabian Sea during the Holocene and the last glaciation. Quat. Res. 36, 72–93. https://doi.org/10.1016/0033-5894(91)90018-Z.
Srivastava, P., Kumar, A., Chaudhary, S., Meena, N., Sundriyal, Y.P., Rawat, S., Rana, N., Perumal, R.J., Bisht, P., Sharma, D., Agnihotri, R., Bagri, D.S., Juyal, N., Wasson, R.J., Ziegler, A.D., 2017. Paleofloods records in himalaya. Geomorphology 284, 17–30. https://doi.org/10.1016/j.geomorph.2016.12.011.
Staubwasser, M., 1999. Early Holocene Variability of the Indian Monsoon and Arabian Sea Thermocline Ventilation. Dissertation thesis. University of Kiel.
Staubwasser, M., Dulski, P., 2002. On the evolution of the oxygen minimum zone in the Arabian Sea during Holocene time and its relation to the South Asian monsoon. Geol. Soc. London, Spec. Publ. 195, 433–443. https://doi.org/10.1144/GSL.SP.2002.195.01.24.
Staubwasser, M., Sirocko, F., 2001. On the formation of laminated sediments on the continental margin off Pakistan: the effects of sediment provenance and sediment redistribution. Mar. Geol. 172, 43–56. https://doi.org/10.1016/S0025-3227(00)00119-5.
Staubwasser, M., Sirocko, F., Grootes, P.M., Erlenkeuser, H., 2002. South Asian monsoon climate change and radiocarbon in the Arabian Sea during early and middle Holocene. Paleoceanography 17. https://doi.org/10.1029/2000PA000608.
Staubwasser, M., Sirocko, F., Grootes, P.M., Segl, M., 2003. Climate change at the 4.2 ka BP termination of the Indus valley civilization and Holocene south Asian monsoon variability. Geophys. Res. Lett. 30. https://doi.org/10.1029/2002GL016822.
Stewart, R.A., Pilkey, O.H., Nelson, B.W., 1965. Sediments of the northern Arabian Sea. Mar. Geol. 3, 411–427. https://doi.org/10.1016/0025-3227(65)90044-7.
Stow, D.A.V., Tabrez, A.R., Prins, M.A., 2002. Quaternary sedimentation on the Makran margin: turbidity current-hemipelagic interaction in an active slope-apron system. Geol. Soc. London, Spec. Publ. 195, 219–236. https://doi.org/10.1144/GSL.SP.2002.195.01.12.
Sun, D., Bloemendal, J., Rea, D.K., Vandenberghe, J., Jiang, F., An, Z., Su, R., 2002. Grain-size distribution function of polymodal sediments in hydraulic and aeolian environments, and numerical partitioning of the sedimentary components. Sediment. Geol. 152, 263–277. https://doi.org/10.1016/S0037-0738(02)00082-9.
Sutherland, H.E., Calvert, S.E., Morris, R.J., 1984. Geochemical studies of the recent sapropel and associated sediment from the Hellenic Outer Ridge, eastern Mediterranean Sea. I: mineralogy and chemical composition. Mar. Geol. 56, 79–92. https://doi.org/10.1016/0025-3227(84)90007-0.
Suthhof, A., Ittekkot, V., Gaye-Hakke, B., 2001. Millennial-scale oscillation of denitrification intensity in the Arabian Sea during the late Quaternary and its potential influence on atmospheric N20 and global climate. Glob. Biogeochem. Cycles 15, 637–649.
Thamban, M., Kawahata, H., Rao, V.P., 2007. Indian summer monsoon variability during the holocene as recorded in sediments of the Arabian Sea: timing and implications. J. Oceanogr. 63, 1009–1020. https://doi.org/10.1007/s10872-007-0084-8.
Tindale, N.W., Pease, P.P., 1999. Aerosols over the Arabian Sea: atmospheric transport pathways and concentrations of dust and sea salt. Deep. Res. Part II Top. Stud. Oceanogr. 46, 1577–1595. https://doi.org/10.1016/S0967-0645(99)00036-3.
von Rad, U., Khan, A.A., Berger, W.H., Rammlmair, D., Treppke, U., 2002. Varves,

turbidites and cycles in upper Holocene sediments (Makran slope, northern Arabian Sea). Geol. Soc. London, Spec. Publ. 195, 387–406. https://doi.org/10.1144/GSL.SP.2002.195.01.21.

von Rad, U., Schaaf, M., Michels, K.H., Schulz, H., Berger, W.H., Sirocko, F., 1999a. A 5000-yr record of climate change in varved sediments from the oxygen minimum zone off Pakistan, northeastern Arabian Sea. Quat. Res. 51, 39–53. https://doi.org/10.1006/qres.1998.2016.

von Rad, U., Schulz, H., Khan, A.A., Ansari, M., Berner, U., Čepek, P., Cowie, G., Dietrich, P., Erlenkeuser, H., Geyh, M., Jennerjahn, T., Lückge, A., Marchig, V., Riech, V., Rösch, H., Schäfer, P., Schulte, S., Sirocko, F., Tahir, M., Weiss, W., 1995. Sampling the oxygen minimum zone off Pakistan: glacial-interglacial variations of anoxia and productivity (preliminary results, sonne 90 cruise). Mar. Geol. 125, 7–19. https://doi.org/10.1016/0025-3227(95)00051-Y.

von Rad, U., Schulz, H., Riech, V., Den Dulk, M., Berner, U., Sirocko, F., 1999b. Multiple monsoon-controlled breakdown of oxygen-minimum conditions during the past 30,000 years documented in laminated sediments off Pakistan. Palaeogeogr. Palaeoclimatol. Palaeoecol. 152, 129–161. https://doi.org/10.1016/S0031-0182(99)00042-5.

von Stackelberg, U., 1972. Faziesverteilung in sedimenten des Indisch-pakistanischen kontinentalrandes (Arabisches Meer). Meteor Forschungsergebnisse, R. C Geol. und Geophys. 9, 1–73.

Walker, M.J.C., Berkelhammer, M., Björck, S., Cwynar, L.C., Fisher, D.A., Long, A.J., Lowe, J.J., Newnham, R.M., Rasmussen, S.O., Weiss, H., 2012. Formal subdivision of the Holocene Series/Epoch: a Discussion Paper by a Working Group of INTIMATE (Integration of ice-core, marine and terrestrial records) and the Subcommission on Quaternary Stratigraphy (International Commission on Stratigraphy). J. Quat. Sci. 27, 649–659. https://doi.org/10.1002/jqs.

Wang, P., Clemens, S., Beaufort, L., Braconnot, P., Ganssen, G., Jian, Z., Kershaw, P., Sarnthein, M., 2005. Evolution and variability of the Asian monsoon system: state of the art and outstanding issues. Quat. Sci. Rev. 24, 595–629. https://doi.org/10.1016/j.quascirev.2004.10.002.

Wanner, H., Solomina, O., Grosjean, M., Ritz, S.P., Jetel, M., 2011. Structure and origin of Holocene cold events. Quat. Sci. Rev. 30, 3109–3123. https://doi.org/10.1016/j.quascirev.2011.07.010.

Wasson, R.J., Smith, G.I., Agrawal, D.P., 1984. Late quaternary sediments, minerals, and inferred geochemical history of Didwana Lake, Thar Desert, India. Palaeogeogr. Palaeoclimatol. Palaeoecol. 46, 345–372. https://doi.org/10.1016/0031-0182(84)90006-3.

Yancheva, G., Nowaczyk, N.R., Mingram, J., Dulski, P., Schettler, G., Negendank, J.F.W., Liu, J., Sigman, D.M., Peterson, L.C., Haug, G.H., 2007. Influence of the intertropical convergence zone on the East Asian monsoon. Nature 445, 74–77. https://doi.org/10.1038/nature05431.